UCSF
UC San Francisco Electronic Theses and Dissertations

Title

Intracellular diffusion in the cytoplasm increases with cell size in fission yeast

Permalink

https://escholarship.org/uc/item/91c421nf

Author

Tan, Catherine

Publication Date

2024

Peer reviewed|Thesis/dissertation

eScholarship.org Powered by the California Digital Library
University of California

Intracellular diffusion in the cytoplasm increases with cell size in fission yeast

by
Catherine Tan

DISSERTATION
Submitted in partial satisfaction of the requirements for degree of
DOCTOR OF PHILOSOPHY

in

Biomedical Sciences

in the

GRADUATE DIVISION
of the
UNIVERSITY OF CALIFORNIA, SAN FRANCISCO

Approved:

DocuSigned by:
Sophie Dumont
8305715E0D454DC...

Sophie Dumont
Chair

DocuSigned by:
Fred Chang
DocuSigned by:

Fred Chang

DocuSigned by:
Abigail Buchwalter Cool
DocuSigned by:

Abigail Buchwalter Cool

DocuSigned by:
68DD18512B3C4D9...

Wallace Marshall

Committee Members

Copyright 2024

by

Catherine Tan

To my past self…

…who thought that getting a PhD was an impossibility…

….and to all those who never did.

Acknowledgements

Firstly, I thank my supervisor, Dr. Fred Chang, who welcomed me in the lab despite that I didn't have any prior biophysics or microscopy experience, who believed in my eagerness to learn physical cell biology, and who allowed me to pursue my naïve ideas during the early years of my PhD. Thank you for always promoting my work to the larger scientific community and for showing me the wonders of Woods Hole year after year. Thank you for supporting me not only as a scientist but as a human being. You've supported my interests beyond the lab, particularly my DEI and activism endeavors. When I struggled personally, you prioritized my well-being, and I never felt that you judged me for my circumstances. Under your mentorship, I found not only intellectual growth but also the freedom to embrace my authentic self.

Of my labmates, I thank Dr. Arthur Molines, Dr. Joël Lemière, and Paula Real Calderon who have been my peers for the entirety of my PhD. Thank you Arthur for providing me the technical foundations of microscopy and image analysis during my first years of grad school. Thank you Joël for continuing to help me develop my technical skills, for talking me off the edge of quitting grad school, and for assuming I could understand the math you tried to teach me. And last, but not least, thank you Paula for answering all my questions on yeast genetics and life in general, and for being the sole reason I came into lab some days because you always made lab fun.

I thank my dissertation committee members Dr. Sophie Dumont, Dr. Wallace Marshall, and Dr. Abigail Buchwalter-Cool for years of mentorship and guidance.

I thank current and past members of HSW6, the Department of Cell and Tissue Biology, MBL Physiology, ASCB-EMBO, the Biomedical Sciences Graduate Program, the

Graduate Division, Scientist 4 Diversity, my rotation labs, my qualifying exam committee, the Multicultural Resource Center, and the United Filipinx Association. Over the years, you fueled my joy for discovery, curated my sense of belonging, and empowered me to be a leader. Thank you all for being part of my PhD journey.

I thank my mentors at the Sanford-Prebys Medical Discovery Research Institute, UCSD, Illumina, and Arima Genomics who helped steer my path towards graduate school.

I thank my parents who financially supported me throughout my academic career, and I thank my extended family members for always being in awe of how “smart” I am.

To those who made San Francisco my home, I thank my close friends Valerie Rosen, Paula Real Calderon, Charlotte Golden, and Donovan Trinidad. Thank you for your unconditional support, kindness, and love throughout these years.

And finally, thank you to Roderick Mendoza for every laugh you’ve given me during those final tough years of grad school.

Intracellular diffusion in the cytoplasm increases with cell size in fission yeast

Catherine Louise Tan

Abstract

Diffusion in the cytoplasm can greatly impact cellular processes, yet regulation of macromolecular diffusion remains poorly understood. There is increasing evidence that cell size affects the density and macromolecular composition of the cytoplasm. Here, we studied whether cell size affects the diffusion of macromolecules in the cytoplasm in the fission yeast *Schizosaccharomyces pombe* cells by analyzing the diffusive motions of intracellular genetically-encoded 40nm nanoparticles (cytGEMs). Using cell size mutants, we found that cytGEMs diffusion coefficients decreased in smaller cells and increased in larger cells. To test if these changes in diffusion rates were due to DNA-to-Cytoplasm (DC) ratio, we used cytokinesis mutants to avoid decreasing DC ratio in large multinucleate cells and found that these cells have comparable cytGEMs diffusion as their normal-sized counterparts. In investigating the underlying causes of altered cytGEMs diffusion, we showed that larger cells have lower concentrations of ribosomal proteins. Finally, comparison of the proteomes of large and small cells defined size-specific changes in the proteome composition. These studies demonstrate that cell size is an important parameter in determining the biophysical properties of the cytoplasm.

Table of Contents

List of Figures

List of Tables

Chapter 1 – Introduction

Cell size is an intrinsic physical property of all cells that can impact physiology from the cellular level to the organismal. Although cell size can vary over six orders of magnitude among diverse cell types, cell size varies within a much narrower range for a specific cell type due to homeostatic mechanisms (Ginzberg *et al.*, 2015; Zatulovskiy and Skotheim, 2020). Cell size can impart different cellular functions and developmental potential (Hecht *et al.*, 2016; Lengefeld *et al.*, 2021). Aberrant cell size can also signify biological dysfunction and has been associated with aging, senescence, numerous cancers, and other human diseases (Lloyd, 2013). The mechanisms for how cell size impacts cellular physiology, however, remain poorly understood.

Recent studies have begun to implicate effects of cell size on the global properties of the cytoplasm. The cytoplasm can be regarded as a heterogenous, dynamic, and crowded viscoelastic matrix that exerts osmotic forces, and impacts nearly all biochemical reactions through effects on viscosity, macromolecular crowding, phase separation, and likely many other biophysical phenomena (Zhou *et al.*, 2008; Mitchison, 2019). For instance, variations in density, which can be the result of complex dynamics between biosynthesis, degradation, and osmotic water fluxes, can cause significant changes in cellular physiology or function as seen during the cell cycle, differentiation, and stress (Neurohr and Amon, 2020).

Generally, the concentrations of cellular components are thought to be maintained at different cell sizes by scaling relationships. For instance, mRNA, protein, transcription, translation, and the volume of many organelles can scale with cell size (Elliott *et al.*, 1979; Creanor and Mitchison, 1982; Elliott, 1983; Neumann and Nurse, 2007; Zhurinsky *et al.*,

2010; Padovan-Merhar *et al.*, 2015; Chadwick *et al.*, 2020; Marshall, 2020; Basier and Nurse, 2023; Swaffer *et al.*, 2023). However, such scaling relationships have limitations, and so, a breakdown in scaling mechanisms could explain cell size-dependent changes in cellular physiology. For example, it was observed that budding yeast cells arrested in G1 phase grew to very large sizes (up to 10 times larger in volume than normal), exhibited defects in protein synthesis, and progressively became less dense (Neurohr *et al.*, 2019). Similar dilution effects have been seen in senescent metazoan cells, indicating that a large cell size may be causal for aspects of senescent physiology, and not merely a side effect (Demidenko and Blagosklonny, 2008; Neurohr *et al.*, 2019; Lengefeld *et al.*, 2021; Lanz *et al.*, 2022). Similarly, in fission yeast, cells arrested in G2 phase grow very large and show a gradual slowdown in rates of cell growth and protein translation, further illustrating that a large cell size is detrimental for proliferation and normal cell function (Knapp *et al.*, 2019a; Basier and Nurse, 2023). For size ranges where overall protein concentration remains relatively constant, recent studies have demonstrated that cell size can also change the composition of the proteome (Schmoller *et al.*, 2015; Keifenheim *et al.*, 2017; Lanz *et al.*, 2022, 2023).

One proposed explanation for certain cellular pathologies associated with overly large cells is that the DNA-to-Cytoplasm (DC) ratio in these cells has dropped below a critical threshold required to scale biosynthetic processes (Zhurinsky *et al.*, 2010; Marguerat and Bähler, 2012; Neurohr *et al.*, 2019; Balachandra *et al.*, 2022; Cadart and Heald, 2022; Xie *et al.*, 2022). As cells grows larger without a concomitant increase in DNA, there may be insufficient transcriptional or translational machinery to support biomass production for an exponentially-growing cell volume. This theory could explain

why diploid and polyploid cells can grow to larger sizes without exhibiting defects associated with large cell size (Neurohr *et al.*, 2019; Mu *et al.*, 2020; Lanz *et al.*, 2022, 2023).

The fission yeast *S. pombe* is a leading model organism in defining cell size control and scaling relationships (Nurse, 1985; Wood and Nurse, 2015). Many studies exploring scaling relationships have used mutants such as *cdc25-22* and *wee1-50*, which alter cell size by affecting the length of G2 phase through regulation of CDK1 cell cycle dependent kinase (Nurse, 1975; Fantes and Nurse, 1978; Neumann and Nurse, 2007; Knapp *et al.*, 2019a; Pickering *et al.*, 2019; Sun *et al.*, 2020). Recent studies show how the intracellular density of the cytoplasm fluctuates during the cell cycle and how properties of the cytoplasm are altered in starvation responses and during sporulation (Joyner *et al.*, 2016; Munder *et al.*, 2016; Heimlicher *et al.*, 2019; Odermatt *et al.*, 2021; Sakai *et al.*, 2023). However, it remains unclear which cellular components are responsible for fluctuations in cytoplasmic density or how the composition of the cytoplasm changes when cell size is altered.

Here, we studied how cell size affects diffusion within the cytoplasm to assess the effects of cell size on the biophysical properties of the cytoplasm. We measured diffusion within living cells by imaging and analyzing the diffusive motion of genetically-encoded multimeric cytoplasmic nanoparticles (cytGEMs), 40 nm-diameter fluorescent particles which inform on the diffusion of macromolecules that are approximately the size of ribosomes (Delarue *et al.*, 2018; Lemière *et al.*, 2022; Molines *et al.*, 2022). We found that diffusion within the cytoplasm increases with increasing cell size in various cell size mutant strains. Using cytokinesis mutants to generate cells that not only became larger,

but also increased their DNA content with cell size thereby preventing a decrease in DC ratio, we find that diffusion does not change in these cells. To gain mechanistic insight into the cell size-dependent rheological effects, we discovered changes in the concentrations of ribosomes and total protein as well as in the composition of the proteome. These size-dependent changes in the physical properties of the cytoplasm provide novel perspectives on the effects of cell size on cellular physiology and function.

Chapter 2 – Intracellular diffusion increases with cell size in fission yeast

2.1 Nanoparticle diffusion in the cytoplasm increases with cell size

To investigate the relationship between cell size and intracellular diffusion, we expressed and imaged 40nm cytGEMs nanoparticles in *S. pombe* wildtype and cell size mutant cells, and through analyses of their motion, determined the effective diffusion coefficient in each strain(Delarue *et al.*, 2018; Lemière *et al.*, 2022; Molines *et al.*, 2022). We grew *wee1-50*, wildtype, and *cdc25-22* cells at the permissive temperature 25°C and shifted to the non-permissive temperature 36°C for six hours before imaging (Fig. 2.1 A) (Nurse, 1975; Fantes and Nurse, 1978). At this temperature, *cdc25-22* cells arrest in G2 phase and continue to grow in length, while *wee1-50* cells exhibit cell cycles with shorter G2 phases and enter mitosis at an abnormally short length. As these rod-shaped cells maintain approximately similar cell widths, the length of the cell was used as an proxy of cellular volume (Mitchison, 1957; Facchetti et al., 2019; Knapp et al., 2019). In our conditions, *wee1-50*, wildtype, and *cdc25-22* cells exhibited an average cell length of 5.61 ± 0.3 μm, 10.84 ± 1.39 μm, and 38.32 ± 1.36 μm, respectively (mean ± STD of replicate experiments). Measurement of the effective diffusion coefficient of cytGEMs in each cell population yielded average cytGEMs effective diffusion coefficients of 0.41 ± 0.04 $\mu m^2/s$ in *wee1-50*, 0.63 ± 0.07 $\mu m^2/s$ in wildtype, and 0.86 ± 0.04 $\mu m^2/s$ in *cdc25-22* cells (Fig. 2.1 B-C; mean ± STD of replicate experiments). Thus, cytGEMs diffusion showed a striking positive correlation between cell size and nanoparticle diffusion in the cytoplasm at the population level. We then analyzed the relationship between cytGEMs diffusion and cell size in individual cells, which exhibited a similar trend of increasing diffusion with cell

size (Fig. 2.2 D). Positive correlations between cell length and cytGEMs diffusion (using a simple linear regression weighted by number of trajectories per cell) were also apparent when analyzing individual cells within *wee1-50* and *cdc25-22* strains (Fig. 2.1 D, Fig. 2.2 A-C), and no correlation was found in wildtype cells (Fig. 2.1 D; Fig. 2.2 B) (Garner *et al.*, 2023).

To address concerns of possible effects of temperature shifts on diffusion and cytoplasmic viscosity, we grew *wee1-50*, wildtype, and *cdc25-22* cells at the permissive and semi-permissive temperatures of 25°C and 28°C, respectively, in steady state conditions (Sidell and Hazel, 1987; Persson *et al.*, 2020; Bellotto *et al.*, 2022). At these temperatures, the mutants generally exhibited detectable but more modest changes in cell size compared to those in the cells shifted to 36°C. At 25°C and 28°C, cytGEMs diffusion rates showed increasing positive trends with cell size across the three strains at the population level (Fig. 2.2 D-G).

To generate large G2-arrested cells using another approach, we inhibited the analog-sensitive CDK1 allele *cdc2-asM17* with the ATP analog drug 1-NM-PP1 at 30°C (Aoi *et al.*, 2014). This treatment leads to G2 arrest and formation of large mononucleate cells, similar to the cdc25 mutants (Fig. 2.1 E). Untreated *cdc2-asM17* cells had an average cell length of 11.32 ± 0.57 μm, while *cdc2-asM17* cells treated with 1-NM-PP1 for 3 hours and 6 hours had average cell lengths of 18.93 ± 0.84 μm and 30.05 ± 3.18 μm, respectively (mean ± STD of replicate experiments). The average cytGEMs diffusion coefficient was 0.42 ± 0.04 $\mu m^2/s$ for control cells, 0.52 ± 0.02 $\mu m^2/s$ for cells treated with 3 hours of 1-NM-PP1, and 0.57 ± 0.02 for cells treated with 6 hours of 1-NM-PP1 (mean ± STD of replicate experiments) (Fig. 2.1 F). Control treatments did not alter cytGEMs

diffusion (Fig. 2.2 G). Overall, these results from a variety of strains and conditions showed a striking positive correlation of intracellular diffusion rates with cell size.

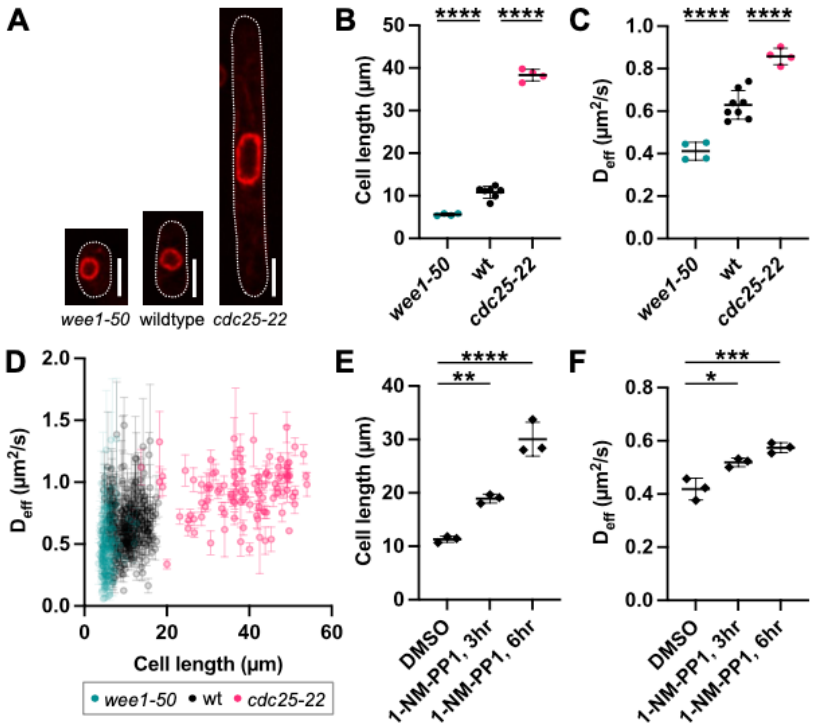

Figure 2.1 Nanoparticle diffusion increases with cell size

(**A**) Images of *wee1-50*, wildtype, and *cdc25-22* cells with nuclear membrane marker Ish1-GFP (red) grown at the permissive temperature 25°C overnight and shifted to the non-permissive temperature 36°C for 6 hours before imaging. Scale bar is 5μm. (**B**) Cell length (mean ± STD of replicate experiments; $N_{CELLS} \geq 106$ per condition from at least 4 biological replicates) (1-way ANOVA, $p < 0.0001$) and (**C**) cytGEMs diffusion (mean ± STD of replicate experiments; $N_{GEMS} \geq 3183$ per condition from at least 4 biological replicates) for *wee1-50*, wildtype, and *cdc25-22* cells grown with the temperature shift protocol described in (**A**) (1-way ANOVA, $p < 0.0001$). (**D**) Cell length and cytGEMs diffusion (mean ± SEM of cytGEMs trajectories per cell; $N_{CELLS} \geq 106$ per condition from at least 4 biological replicates) plotted for individual cells for *wee1-50*, wildtype, and *cdc25-22* cells grown with the temperature shift protocol described in (**A**). (**E**) Cell length (mean ± STD of replicate experiments; $N_{CELLS} \geq 113$ per condition from 3 biological replicates) and (**F**) cytGEMs diffusion (mean ± STD of replicate experiments; $N_{GEMS} \geq 5709$ per condition from 3 biological replicates) for *cdc2-asM17* cells treated with 0.25% DMSO or 10μM ATP analog 1-NM-PP1. (1-way ANOVA, * - $p < 0.05$, ** - $p < 0.01$, *** - $p < 0.001$, **** - $p < 0.0001$).

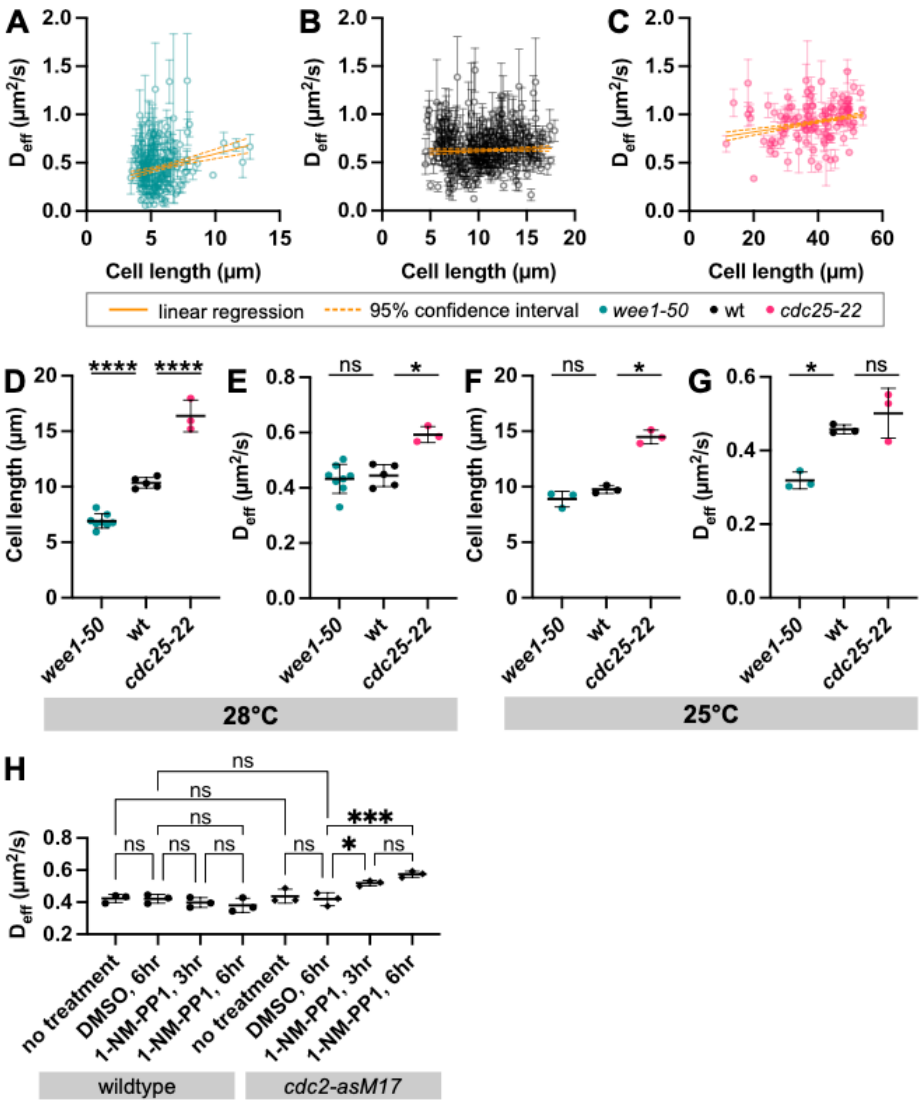

Figure 2.2 Supporting data for Figure 2.1

(**A**) Cell length and cytGEMs diffusion (mean ± SEM of cytGEMs trajectories per cell) plotted for individual cells for *wee1-50*, (**B**) wildtype, and (**C**) *cdc25-22* cells grown with the temperature shift protocol described in Figure 1A. Weighted linear regression (orange solid line) with 95% confidence interval (orange dashed lines) shown. Best-fit slopes are 0.03, 0.003, and 0.005 for (**A**), (**B**), and (**C**), respectively. (**D**) Cell length and (**E**) cytGEMs diffusion (mean ± STD of replicate experiments; $N_{GEMS} \geq 5135$ per condition from at least 3 biological replicates) for *wee1-50*, wildtype, and *cdc25-22* cells grown at the steady-state semi-permissive temperature 28°C. (**F**) Cell length and (**G**) cytGEMs diffusion (mean ± STD of replicate experiments; $N_{GEMS} \geq 5981$ per condition from at least 3 biological replicates) for *wee1-50*, wildtype, and *cdc25-22* cells grown at the steady-state permissive temperature 25°C. (**H**) CytGEMs diffusion (mean ± STD of replicate experiments) in wildtype and *cdc2-asM17* cells with varying conditions of 0.25% DMSO and 10μM 1-NM-PP1. (1-way ANOVA, * - $p < 0.05$, *** - $p < 0.001$, **** - $p < 0.0001$).

2.2 Large multinucleate cells maintain nanoparticle diffusion

To determine whether the increase in cytGEMs diffusion in larger cell sizes was due to a decrease in the DNA-to-Cytoplasm (DC) ratio, we analyzed large multinucleated fission yeast cells in which the DC ratio does not decrease. We generated these multinucleate cells using well-established mutants *sid2-as* and *cdc11-119* that are defective in the SIN regulatory pathway of cytokinesis (Nurse *et al.*, 1976; Grallert *et al.*, 2012). These conditional mutants continue to grow in length and undergo nuclear division cycles in the absence of septation. *Sid2-as* cells treated with the ATP analog 1-NM-PP1 formed progressively larger cells with multiple nuclei at three and six hours of treatment (Fig. 2.3 A-C). Control *sid2-as* cells had an average cell length of 10.36 ± 0.34 μm while *sid2-as* cells treated with 1-NM-PP1 for 3 hours and 6 hours had average cell lengths of 16.55 ± 0.91 μm and 25.95 ± 1.6 μm, respectively (mean ± STD of replicate experiments). Based on the average cell length and number of nuclei per condition, we estimated that the DC ratio of 1-NM-PP1-treated cells did not decrease compared to the control. Despite being larger in cell size, we found that cytGEMs diffusion coefficients in treated *sid2-as* cells (3 hours: 0.48 ± 0.6 μm2/s; 6 hours: 0.56 ± 0.01 $\mu m^2/s$) were comparable with the control cells (0.52 ± 0.04 $\mu m^2/s$) (mean ± STD of replicate experiments) (Fig. 2D).

Next, we inhibited cytokinesis by using the temperature-sensitive mutant *cdc11-119* (Nurse *et al.*, 1976). Wildtype cells and *cdc11-119* cells were grown at the permissive temperature 25°C overnight and shifted to the non-permissive temperature 36°C for 3 hours. We observed a comparable cytGEMs diffusion coefficient in the *cdc11-119* cells compared to control populations (Fig. 2.4 B). Overall, these results suggest that a

decrease in DC ratio rather than an increase in cell size alone, underlies the increase in intracellular diffusion observed in large cells (Fig. 2.1).

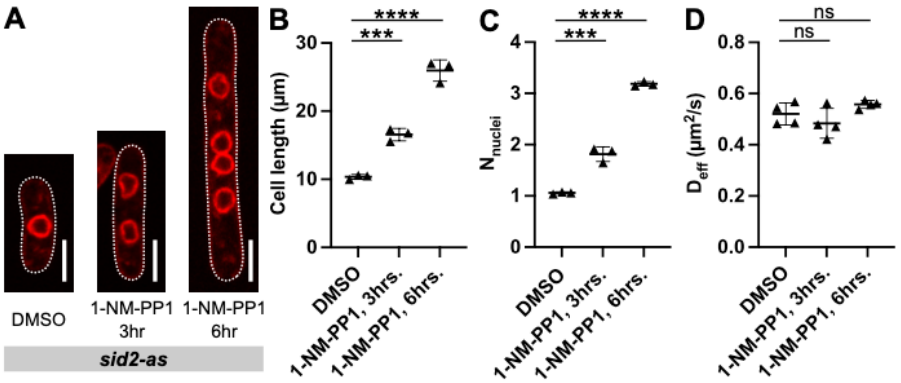

Figure 2.3 Large multinucleate cells maintain nanoparticle diffusion rates

(**A**) Images of *S. pombe sid2-as* cells with nuclear membrane marker Ish1-mScarlet (red). Cells were grown at steady-state 30°C and treated with 0.25% DMSO or 10μM ATP analog 1-NM-PP1. Left to right: 6hr DMSO, 3hr 1-NM-PP1, and 6hr 1-NM-PP1. Scale bar is 5μm. (**B**) Cell length, (**C**) number of nuclei (mean ± STD of replicate experiments; N_{CELLS} ≥ 140 per condition from 3 biological replicates), and (**D**) cytGEMs diffusion (mean ± STD of replicate experiments; N_{GEMS} ≥ 5546 per condition from 4 biological replicates) for *sid2-as* cells described in (**A**). (1-way ANOVA, *** - $p < 0.001$, **** - $p < 0.0001$).

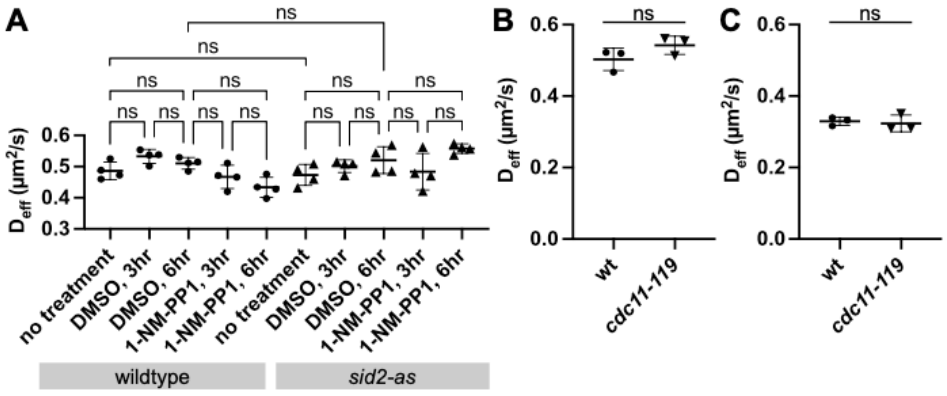

Figure 2.4 Supporting data for Figure 2.3

Supplementary Figure 2. Large multinucleate cells maintain nanoparticle diffusion rates. (**A**) CytGEMs diffusion (mean ± STD of replicate experiments) in wildtype and *sid2-as*
(Figure caption continued on the next page.)

Figure 2.4 Supporting data for Figure 2.3

(Figure caption continued from the previous page.) cells with varying conditions of 0.25% DMSO and 10μM 1-NM-PP1 (1-way ANOVA, $p > 0.05$). (**B**) CytGEMs diffusion (mean ± STD of replicate experiments; $N_{GEMS} \geq 7630$ per condition from 3 biological replicates) for wildtype and *cdc11-119* cells grown at permissive temperature 25°C overnight and shifted to the non-permissive temperature 36°C for 3 hours before imaging (Komogorv-Smirnov test, $p = 0.6$). (C) CytGEMs diffusion (mean ± STD of replicate experiments; $N_{GEMS} \geq 9782$ per condition from 3 biological replicates) for wildtype and *cdc11-119* cells grown at the steady-state permissive temperature 25°C (Komogorv-Smirnov test, $p = 0.6$).

2.3 Ribosomal and total protein concentrations decrease in large cells

We hypothesized that the cell size-dependent changes in cytGEMs diffusion reflect changes in cytoplasmic composition or concentration. Previous studies suggest that such changes may correlate with a decrease in ribosome concentration or overall protein concentration (Delarue *et al.*, 2018; Neurohr *et al.*, 2019). To assess ribosomal concentration, we measured the fluorescence intensity of Rps2-GFP, a functional fusion of the essential small subunit ribosomal protein expressed at the native locus (Knapp et al., 2019; Lemière et al., 2022). *Wee1-50*, wildtype, and *cdc25-22* cells expressing Rps2-GFP were grown at the permissive temperature 25°C overnight and shifted to the non-permissive temperature 36°C for 6 hours before imaging (Fig. 2.5 A). To facilitate equivalent processing, cells of the three strains were mixed, stained together, and imaged in the same field. We found a distinct inverse relationship of Rps2 intensity with cell size (Fig. 2.5 B). In binned data, the average intensity of Rps2-GFP was significantly lower in bigger cells (cell length ≥ 18 μm) compared to medium-sized cells (cell length between 9 and 18 μm), but no significant differences were detected between medium and smaller cells (cell length ≤ 9 μm) (Fig. 2.5 B-C).

To assess overall protein concentration, we measured the intensity of fluorescent dye fluorescein isothiocyanate (FITC) staining in fixed cells (Fig. 2.5 D). *Wee1-50*, wildtype, and *cdc25-22* cells were shifted to 36°C for 6 hours, mixed, fixed, stained with FITC, and imaged. In binned data, compared to medium-sized cells, FITC intensity was about 6% lower in bigger cells (p=0.04) and 5% lower in smaller cells (not significant). These results were consistent with an overall decrease in dry mass density seen previously in cdc25-25 cells (Odermatt *et al.*, 2021).

Overall, our results showed that larger cells exhibited a decrease in ribosomal protein concentration and to a lesser extent, overall protein concentration, which begin to provide an explanation for the increase in cytGEMs mobility with increasing cell size.

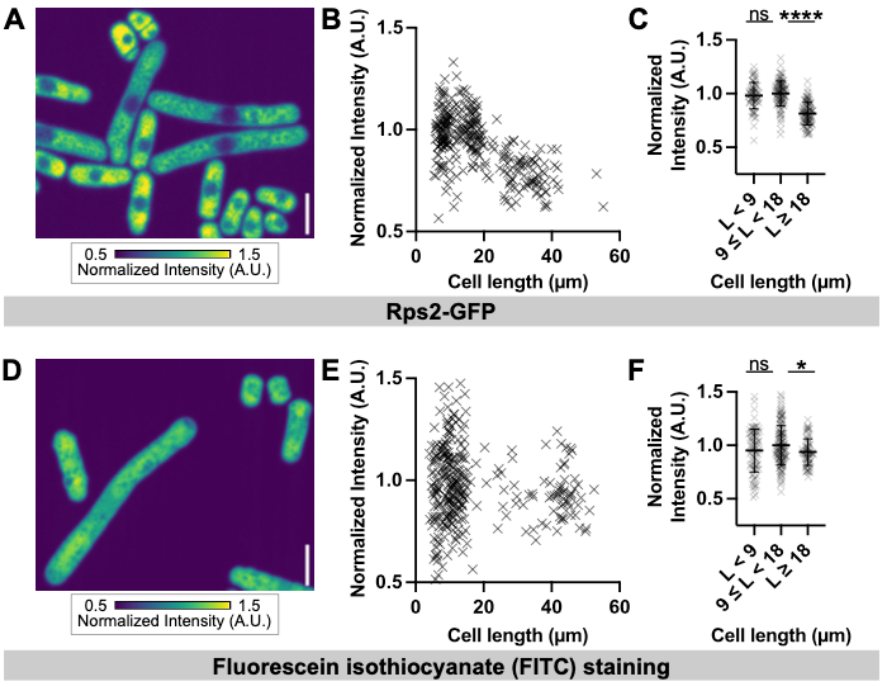

Figure 2.5 Large cells have decreased concentrations of ribosomes and overall protein content

(**A**) Image of a mixture of *wee1-50*, wildtype, and *cdc25-22* live cells with ribosomal protein marker Rps2-GFP. Scale bar is 5μm. (**B**) Rps2-GFP intensity and length per cell. (Figure caption continued on the next page.)

Figure 2.5 Large cells have decreased concentrations of ribosomes and overall protein content

(Figure caption continued from the previous page.) (**C**) Rps2-GFP intensities (mean ± STD per cell length category; $N_{CELLS} \geq 72$ per condition from 3 biological replicates) measured in a mixture of *wee1-50*, wildtype, and *cdc25-22* cells and categorized by cell length. (**D**) Image of a mixture of *wee1-50*, wildtype, and *cdc25-22* fixed cells, treated with RNase A, and stained with FITC. (**E**) FITC intensity and length per cell. (**F**) FITC intensities (mean ± STD per length category; $N_{CELLS} \geq 73$ per condition from 3 biological replicates) measured in a mixture of *wee1-50*, wildtype, and *cdc25-22* fixed cells and categorized by cell length. Intensity values for Rps2-GFP and FITC are normalized to the mean intensity of the $9 \leq L < 18$ category (1-way ANOVA test, * - $p < 0.05$, **** - $p < 0.0001$).

2.4 Proteome composition varies with cell size

To investigate how the composition of the cytoplasm changes with cell size, we characterized the proteomes of *S. pombe wee1-50*, wildtype, and *cdc25-22* cells grown under various conditions. Mass spectrometry was analyzed using SILAC in pairwise comparisons. First, *cdc25-22* and *wee1-50* SILAC strains were labeled with the lysine and arginine isotopes at the permissive temperature 25°C overnight and shifted to the non-permissive temperature 36°C for six and half hours before peptide extraction, which produced similar size ranges to the *cdc25-22* and *wee1-50* cell populations analyzed in Figure 2.1. Proteomic analyses detected 3,353 proteins out of 5,117 identified *S. pombe* proteins (~65% coverage), and our two experimental repetitions yielded consistent results (R=0.83, Pearson) (Fig. 2.6 A). We categorized proteins by their subcellular location or macromolecular complex such as histones (magenta), ribosomes (orange), and ER (cyan) (Fig. 2.6 A). Finally, we grouped proteins by their subcellar location or macromolecular complex and averaged their collective ratios (Fig. 2.6 B). Because relative concentrations of each protein were calculated and normalized within each strain,

we note that these analyses cannot reveal alterations in real protein concentrations but only relative changes to other proteins.

Overall, we observed differential scaling of proteins in comparing large and small cell proteomes. Proteins associated with the nucleus including the nucleolus, histones (magenta, out of range), and chromosome sub-scaled with cell size, i.e. they were underrepresented in the large *cdc25-22* cells compared to small *wee1-50* cells (Fig. 2.6 B, red quadrant). This sub-scaling behavior was expected, as chromosome-associated proteins such as histones are known to scale with DNA content, not cell size (Claude *et al.*; Amodeo *et al.*, 2015). Notably, ribosomal proteins (Fig. 2.6 B, orange) also exhibited sub-scaling, which supported our observation that ribosome concentration is decreased in these large cells (Fig. 2.6 A-C). Overall, cytoplasmic proteins are also sub-scaling with cell size. In contrast, proteins associated with the endoplasmic reticulum (cyan), mitochondria, and vacuoles super-scaled with cell size, i.e. they were overrepresented in the large *cdc25-22* cells compared to small *wee1-50* cells (Fig. 2.6 B, blue quadrant).

Next, we examined the proteome data for scaling of cellular processes and signaling pathways implicated in regulation of cytoplasmic properties in other studies. One candidate signaling pathway that regulates ribosome concentration and stress responses is the TORC1 pathway (Delarue *et al.*, 2018). Proteins associated with TORC complexes and ribosome biogenesis sub-scaled with cell size (Fig. 2.7 A). To test whether TORC1 activity is decreased in large cells, we found that factors downstream of the Sfp1 transcription factor also sub-scaled with size (Tai *et al.*, 2023). However, in contrast to other studies characterizing cell size proteome changes (Neurohr *et al.*, 2019; Lanz *et al.*, 2022, 2023), we detected no significant super-scaling effects on stress-associated

pathways such as the core environmental stress response (CESR) (Chen *et al.*, 2003). As levels of the viscogen trehalose may be an additional mechanism to regulate cytoplasmic viscosity that is independent of ribosome concentration, we found that proteins involved in trehalose biosynthesis sub-scaled with size and those associated with trehalose breakdown super-scaled with size (Fig. 2.7 A) (Persson *et al.*, 2020). To analyze the top hits for sub- and super-scaling proteins in our data set, we performed a gene ontology enrichment analysis (PANTHER overrepresentation test) (Fig. 2.7 B). Top super-scaling proteins were generally involved in metabolic pathways associated with membrane-bound organelles, whereas top sub-scaling proteins were associated with cell polarity regulation at cell tips, and mRNA regulation and gene expression in the nucleus. Of interest, among the sub-scaling cell polarity proteins was the DYRK protein kinase Pom1 as well its regulators Tea1 and Tea4, which all localize to cell tips and contribute to cell size sensing for cell size regulation (Martin and Berthelot-Grosjean, 2009; Moseley *et al.*, 2009; Hachet *et al.*, 2011; Wood and Nurse, 2015).

Additional proteomic comparisons between cells with smaller size differences supported these results. First, comparison of *cdc25-22* and wildtype cells, grown with the temperature shift protocol described in Fig. 2.6 , showed similar trends as our comparison between *cdc25-22* and *wee1-50* cells (Fig. 2.8 A-B). Second, we compared *cdc25-22* and *wee1-50* strains grown at steady-state at 28°C (similar to Fig. 2.2 D-E) to remove effects of temperature shift. Here, we observe the same general trends in the proteome, with the notable exception of ribosome proteins which scaled with cell size in these conditions (Fig. 2.8 C-D).

Overall, our data revealed that the proteome has characteristic composition changes with cell size and indicate that ribosomal proteins and certain nuclear proteins were less abundant in large cells relative to other sets of proteins, such as those associated with membrane organelles. Our data were consistent with the recent cell size findings in budding yeast and mammalian proteomes, demonstrating that these are likely to be general signatures of cell size (Fig. 2.7 C) (Lanz *et al.*, 2022, 2023). In general, these results begin to demonstrate how remodeling of the composition of the cytoplasm lead to changes in diffusion in cells of varying sizes.

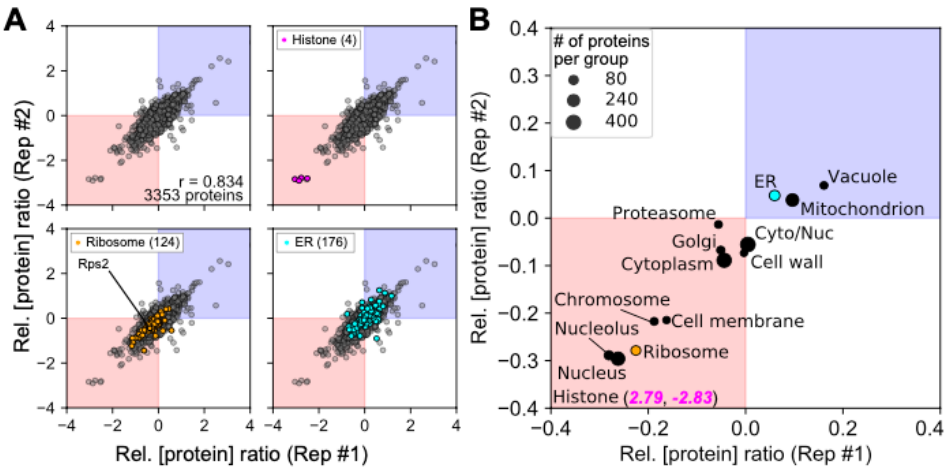

Figure 2.6 Proteome composition varies with cell size

Two replicates of SILAC proteomics experiments were performed on *cdc25-22* and *wee1-50* cells grown with temperature shift. Concentrations of each protein are determined per strain and normalized to the respective strain's proteome. To compare proteome differences between *cdc25-22* and *wee1-50*, these relative concentration ratios were expressed as a ratio of *cdc25-22*/*wee1-50*. (**A**) Relative protein concentration ratios (*cdc25-22*/*wee1-50*) for each detected protein. Proteins highlighted according to select subcellular locations. Number of proteins per subcellular location category in parentheses. Upper right quadrant (blue) indicates proteins that have relative protein concentration ratios that are more than 1. These proteins are relatively more abundant in *cdc25-22* compared to *wee1-50*. By contrast, the lower left quadrant (red) indicates proteins that have relative protein concentration ratios that are less than 1. These proteins are relatively less abundant in *cdc25-22* compared to *wee1-50*. (**B**) Average relative concentration ratios of proteins grouped by subcellular localization.

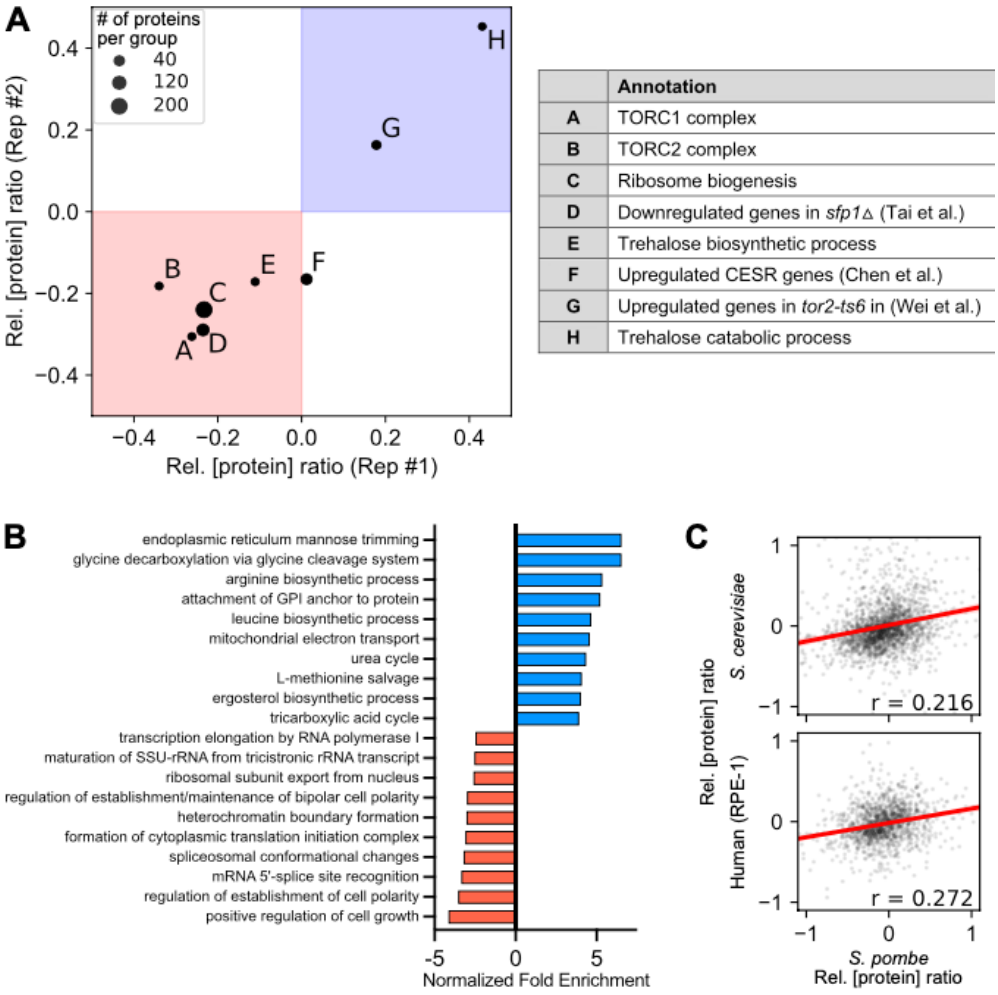

	Annotation
A	TORC1 complex
B	TORC2 complex
C	Ribosome biogenesis
D	Downregulated genes in *sfp1*Δ (Tai et al.)
E	Trehalose biosynthetic process
F	Upregulated CESR genes (Chen et al.)
G	Upregulated genes in *tor2-ts6* in (Wei et al.)
H	Trehalose catabolic process

Figure 2.7 Comparison of *S. pombe* proteome size scaling with other studies

(**A**) Average relative concentration ratios of proteins grouped by biological processes for *S. pombe* (*cdc25-22*/*wee1-50* grown with temperature shift). Biological processes were selected based on prior evidence that the biological process affects diffusion of nanoparticles or has been associated with cytoplasmic dilution. (**B**) Gene ontology analysis of sub- (red) and super-scaling (blue) proteins in *S. pombe* (*cdc25-22*/*wee1-50* grown with temperature shift). (**C**) Correlations between size-scaling proteomics datasets of *S. pombe* (*cdc25-22*/*wee1-50* grown with temperature shift) compared to (top) S. cerevisae (from Lanz et al. 2023, cell size mutants) and (bottom) human RPE-1 cells (from Lanz et al. 2022., size-sorted).

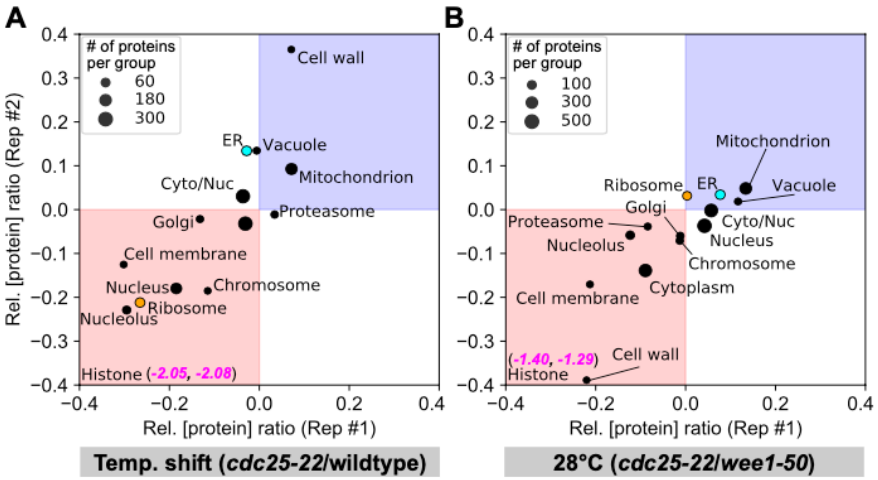

Figure 2.8 Cell size proteome remodeling is observed at smaller cell size differences

Cell size proteome remodeling is observed at smaller cell size differences. (**A**) Average relative protein concentration ratios (*cdc25-22*/wildtype) of proteins grouped by subcellular localization. Cells are grown at the permissive temperature 25°C overnight and shifted to the non-permissive temperature 36°C for 6.5 hours (approximately two doublings) before sample collection. (**B**) Average relative concentration ratios (*cdc25-22*/*wee1-50*) proteins grouped by subcellular localization. Cells are grown at steady-state 28°C.

Chapter 3 – Additional unpublished data

3.1 Intracellular diffusion in the nucleus increases with cell size

To investigate whether the phenomenon of diffusion increasing with cell size occurs not only in the cytoplasm, but also in the nucleus, we expressed and imaged 40nm nucGEMs nanoparticles in *S. pombe* wildtype and the cell size mutant cells *wee1-50* and *cdc25-22* (Szórádi *et al.*; Lemière *et al.*, 2022). Similar to Fig. 2.1, we grew *wee1-50*, wildtype, and *cdc25-22* cells at the permissive temperature 25°C and shifted to the non-permissive temperature 36°C for six hours before imaging (Nurse, 1975; Fantes and Nurse, 1978). Each cell population yielded average effective nucGEMs diffusion coefficients of 0.48 ± 0.05 $\mu m^2/s$ in *wee1-50*, 0.63 ± 0.04 $\mu m^2/s$ in wildtype, and 0.81 ± 0.03 $\mu m^2/s$ in *cdc25-22* cells (Fig. 3.1 A; mean ± STD of replicate experiments). Thus, nucGEMs diffusion showed a striking positive correlation between cell size and nanoparticle diffusion in the nucleus at the population level. We then analyzed the relationship between nucGEMs diffusion and cell size in individual cells, which exhibited a similar trend of increasing diffusion with cell size (Fig. 3.1 B). Overall, our data show that diffusion increases with cell size both in the cytoplasm and the nucleoplasm. This suggests that, as cells grow large, both compartments may experience biophysical changes, such as a “dilution” of macromolecules, and can have profound effects on processes that occur in either compartment.

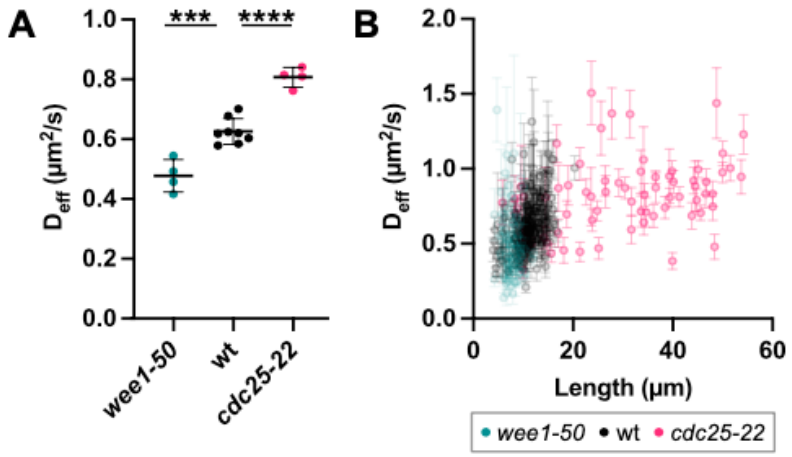

Figure 3.1 Nanoparticle diffusion in the nucleus increases with cell size

(**A**) nucGEMs diffusion (mean ± STD of replicate experiments) for *wee1-50*, wildtype, and *cdc25-22* cells grown with the temperature shift protocol described in Fig. 2.1 A (1-way ANOVA, $p < 0.0001$). (**B**) Cell length and nucGEMs diffusion (mean ± SEM of nucGEMs trajectories per cell; $N_{CELLS} \geq 72$ per condition from at least 4 biological replicates) plotted for individual cells for *wee1-50*, wildtype, and *cdc25-22* cells grown with the temperature shift protocol described in (**A**). (1-way ANOVA, * - $p < 0.05$, ** - $p < 0.01$, *** - $p < 0.001$, **** - $p < 0.0001$).

3.2 Inhibiting ribosomal biogenesis may be sufficient to alter intracellular diffusion in fission yeast

Ribosomes have been identified as a crowding agent in the cytoplasm in budding yeast and human cell lines as treating these cells with rapamycin, an TOR inhibitor, resulted in decreased ribosomal concentration and increased diffusion in the cytoplasm (Delarue *et al.*, 2018). Additionally, deletion of the positive ribosome biogenesis transcriptional regulator Sfp1 also results in an cytGEMs diffusion increase in budding yeast (Delarue *et al.*, 2018). Although we observe a concurrent decrease in ribosomal concentration and an increase in cytGEMs diffusion in very large fission yeast cells (Fig. 2.1 and 2.5), it was unclear whether decreasing ribosomal concentration, without greatly increasing cell size, would also result in increased intracellular diffusion.

We observed protein scaling behaviors in large fission yeast cells that were consistent with ribosome biogenesis inhibition, either through mutants that inhibited TOR function or had a Sfp1 deletion (Fig. 2.6 A). To test whether inhibition of ribosome biogenesis is sufficient to increase diffusion of GEMs, we first measured GEMs diffusion in cells that were treated with Rbin-1, a specific inhibitor of Midasin, an ATPase involved in the assembly of nucleolar precursors of the ribosome 60S subunit (Kawashima *et al.*, 2016). After 2 hours of 10μM Rbin-1 treatment, 60S precursors accumulate in the nucleus (Fig. 3.2 A), and we observed that diffusion the cytoplasm increases (DMSO: 0.56 ± 0.07 $\mu m^2/s$; Rbin-1: 0.75 ± 0.01 $\mu m^2/s$) and diffusion the nucleus decreases (DMSO: 0.75 ± 0.01 $\mu m^2/s$; Rbin-1: 0.58 ± 0.05 $\mu m^2/s$) (Fig. 3.2 BC; mean ± STD of replicate experiments). Next, we treated cells with 1hour of 25μM Torin1, a TOR inhibitor that inhibits both TORC1 and TORC2 in fission yeast. Here, did not observe a significant change in diffusion in the cytoplasm (DMSO: 0.51 ± 0.07 $\mu m^2/s$; Torin1: 0.53 ± 0.03 $\mu m^2/s$), though we did see a modest increase in diffusion in the nucleus (DMSO: 0.52 ± 0.00 $\mu m^2/s$; Torin1: 0.59 ± 0.03 $\mu m^2/s$) (Fig. 3.2 DE; mean ± STD of replicate experiments). Finally, we measured nucGEMs diffusion in cells with an Sfp1 deletion and observed a significant increase in diffusion in the nucleus (wt: 0.45 ± 0.00 $\mu m^2/s$; *sfp1*△*:* 0.54 ± 0.03 $\mu m^2/s$) (Fig. 3.2 F; mean ± STD of replicate experiments). Overall, these data suggest that intracellular diffusion can be altered by inhibiting ribosome biogenesis with various methods thereby further implicating ribosomes as a crowding agent in fission yeast.

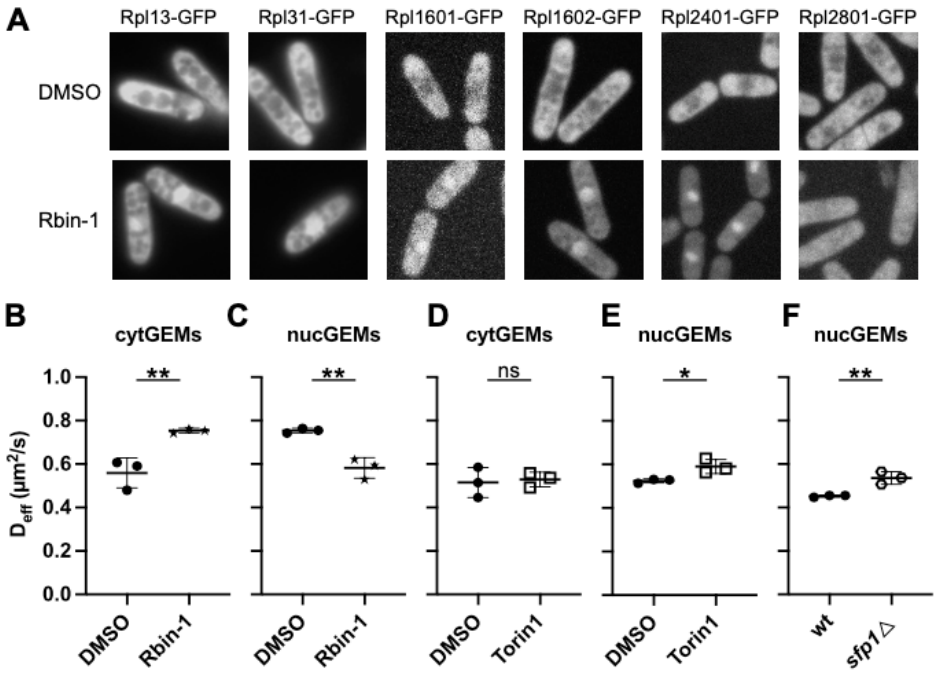

Figure 3.2 Inhibiting ribosomal biogenesis may be sufficient to alter intracellular diffusion

(**A**) Images of *S. pombe* wildtype cells with various ribosomal proteins tagged with GFP treated with 0.5% DMSO or 10μM Rbin-1 for 2 hours at 30°C. (**B**) CytGEMs and (**C**) nucGEMs diffusion (mean ± STD of replicate experiments; $N_{CELLS} \geq 55$ and $N_{GEMS} \geq 1118$ per condition from 3 biological replicates) of wildtype cells treated with DMSO and Rbin-1 as described in (**A**). (**D**) CytGEMs and (**E**) nucGEMs diffusion (mean ± STD of replicate experiments; $N_{CELLS} \geq 65$ and $N_{GEMS} \geq 1488$ per condition from 3 biological replicates) of wildtype cells treated with 1% DMSO and 25μM Torin1 for 1 hour at 30°C. (**F**) NucGEMs diffusion (mean ± STD of replicate experiments; $N_{CELLS} \geq 68$ and $N_{GEMS} \geq 1668$ per condition from 3 biological replicates) of wildtype and *sfp1*△ cells. Unpaired t-test, * - $p < 0.05$, ** - $p < 0.01$).

Chapter 4 – Discussion

Here, we demonstrate that intracellular diffusion coefficients of macromolecular-sized particles show a significant positive correlation with increasing cell size. Relative to wildtype cells, cytGEMs diffusion increased in large *cdc25-22* mutant cells and decreased in the smaller *wee1-50* mutant cells (Fig. 2.1). However, cytGEMs diffusion was not changed in large multinucleate cells, demonstrating that DNA-to-Cytoplasm (DC) ratio may be the critical parameter that underlies diffusion rates rather than cell size alone (Fig. 2.3). In investigating the mechanism underlying these changes in diffusion, we showed that large and small cells exhibited different proteome compositions, with large cells exhibiting decreased concentrations of ribosome and nuclear proteins relative to other elements of the proteome. These results are consistent with a model in which diffusion increases in larger cells due to a decrease in the concentration of ribosomes and changes to the concentrations of many other cytoplasmic components. In proliferating cells, a limiting factor may be the number of gene copies needed to maintain gene expression to support the exponential growth of the cytoplasm (Zhurinsky *et al.*, 2010; Marguerat and Bähler, 2012; Neurohr *et al.*, 2019; Balachandra *et al.*, 2022; Cadart and Heald, 2022; Xie *et al.*, 2022).

Overall, our study supports the premise that the properties of the cytoplasm vary at different cell sizes. While previous studies focus on the apparent dilution of the cytoplasm and/or changes in the biochemical composition in large cells (Neurohr *et al.*, 2019; Lanz *et al.*, 2022), our findings show that cell size impacts diffusion and crowding in the cytoplasm. As diffusion and crowding have broad range effects on the inner workings of the cell, including the rates of most biochemical reactions, our findings

introduce a critical component in our understanding of the effects of cell size on cellular physiology.

Our studies leverage certain advantages in the fission yeast model. The use of the cytGEMs nanoparticle is well-established as a quantitative tool in these cells (Lemière *et al.*, 2022; Molines *et al.*, 2022). In using well-studied cell cycle mutants, the molecular bases for the perturbations in cell size and genomic copy number are defined (Nurse, 1975; Nurse *et al.*, 1976; Fantes and Nurse, 1978; Hagan *et al.*, 2016). Rather than using polyploid or endoreplication lines that may have the specific effects on cellular physiology, we used well-characterized cytokinesis mutants to transiently produce large multinucleate cells (Neurohr *et al.*, 2019; Lanz *et al.*, 2022). Because of the abilities to determine cell size of individual cells, our study utilized single-cell analyses in addition to bulk population measurements. Although surface area-to-volume (SA/V) ratio can impose constraints on metabolism across cell sizes, SA/V ratios do not vary with cell size in our cells due to the characteristic rod-cell shape of fission yeast used in this study (Shi et al., 2021). The observed changes in cytGEMs diffusion are consistent with a previous study that highlighted the cell cycle-dependent fluctuations in intracellular density where cell density decreases during G2 phase and increases during cell division (Odermatt *et al.*, 2021). One mechanism for density dilution in *cdc25-22* arrested cells may be due to the prolonged time in G2 phase when the rate of volume growth slightly outpaces mass biosynthesis. By contrast, the density increase in *wee1-50* cells may be due to the enrichment of dividing cells in the *wee1-50* population.

In addition, our studies contribute to a growing body of evidence that the cytoplasm not only becomes more dilute with increasing cell size, but also, that composition of the

cytoplasm remodels with cell size. Comparison of our results with recent data in human cells and budding yeast cells show that this remodeling of the proteome is largely conserved in these eukaryotic cells (Fig. 2.7) (Lanz *et al.*, 2022, 2023). For example, in these three organisms, our studies agree in that sub-scaling proteins are enriched in nuclear proteins, while super-scaling proteins are enriched in ER and mitochondrial proteins as well as metabolic proteins (Fig. 2.6). Proteome remodeling in budding yeast is thought to be independent of metabolic state, but holds similarities to cells in the starvation state and during environmental stress response (Lanz *et al.*, 2023). However, we did not detect these similarities for fission yeast (Fig. 2.7 A). Our proteome and fluorescence intensity analyses (Fig. 2.5, 2.7) together showed that the concentration of ribosomal proteins subscales in larger fission yeast cells. As ribosomes have been suggested to be the primary crowding agent of macromolecules in the cytoplasm, the decrease in not only ribosomal protein concentration but also the decrease in ribosome biogenesis proteins and TOR complex proteins altogether provide a possible mechanism for increased diffusion mediated through the TOR pathway (Delarue *et al.*, 2018).

In addition to ribosomal concentration, it is likely that other factors also contribute to cell size effects. We noted that ribosomal protein and protein content alone cannot readily account for all the diffusion data; for instance, we detected no significant decrease in ribosomal protein concentration associated with increased diffusion in *wee1-50* cells (Fig. 2.1, 2.2, 2.5). Therefore, there are likely to be additional factors that contribute to diffusion changes, such as small viscogens like trehalose and glycerol (Fig. 2.7).

Changes in macromolecular crowding and diffusion are predicted to have significant impact on the biochemistry and mechanobiology inside the cell. For instance,

these physical cytoplasmic properties not only affect rates of biochemical reactions, dynamics of molecular conformational changes, and protein expression, but they also impact organelle size and phase transitions that help to organize the cytoplasm (Rivas and Minton, 2016; Mitchison, 2019; Marshall, 2020). Our studies suggest that one reason why cell size is maintained in a homeostatic manner is to maintain the state of the cytoplasm. In abnormally-sized cells seen in senescence, aging, or disease states, altered cytoplasmic properties may contribute to slower growth rates, abnormal cellular function, and cell death (Neurohr and Amon, 2020; Xie *et al.*, 2022). Future studies promise to reveal how cell size affects the intracellular environment responsible for cellular functions.

Chapter 5 – Methods and Materials

Table 5.1 Key resources used in this study

Reagent type (species) or resource	Designation	Source or reference	Identifiers	Additional Information
Genetic reagent (*Schizosaccharomyces pombe*)	Ish1-mScarlet	Chang Lab collection	FC 3318	*h- ade6<<mCherry-psy1 ish1-GFP:kanMX ura4-D18*
Genetic reagent (*S. pombe*)	Ish1-mScarlet, *cdc25 mutant*	This manuscript	FC 3339	*cdc25-22 ade6<<mCherry-psy1 ish1-GFP:kanMX*
Genetic reagent (*S. pombe*)	Ish1-mScarlet, *wee1 mutant*	This manuscript	FC 3340	*wee1-50 ish1-GFP:kanMX*
Genetic reagent (*S. pombe*)	cytGEMs	Chang Lab collection	FC 287	*h- pREP41X-PfV-Sapphire leu1-32*
Genetic reagent (*S. pombe*)	cytGEMs, *cdc25* mutant	This manuscript	FC 3341	*h+ cdc25-22, pREP41X-PfV-Sapphire leu1-32*
Genetic reagent (*S. pombe*)	cytGEMs, *wee1* mutant	This manuscript	FC 3342	*h- wee1-50, pREP41X-PfV-Sapphire leu1-32 hist?*
Genetic reagent (*S. pombe*)	cytGEMs, *cdc2* mutant	This manuscript	FC 3343	*h90 cdc2-asM17, pREP41X-PfV-Sapphire, leu1-32, ura4-D18*
Genetic reagent (*S. pombe*)	cytGEMs, *sid2* mutant, ish1-mScarlet	This manuscript	FC 3344	*h+ sid2-as ish1:mScarlet-I:hphMX6 ade6-M210, pREP41X-PfV-Sapphire, leu1-32 ura4-D18*
Genetic reagent (*S. pombe*)	cytGEMs, *cdc11* mutant	This manuscript	FC 3345	*h- cdc11-119, pREP41X-PfV-Sapphire leu1-32*
Genetic reagent (*S. pombe*)	Rps2-GFP	Chang Lab collection	FC3209	*h- rps2-GFP::kanR leu1-32 ura4-D18 ade6-210*
Genetic reagent (*S. pombe*)	Rps2-GFP, *cdc25* mutant	This manuscript	FC 3346	*cdc25-22 rps2-GFP::kanR leu1-32 ura4-D18*
Genetic reagent (*S. pombe*)	Rps2-GFP, *wee1* mutant	This manuscript	FC 3347	*wee1-50 rps2-GFP::kanR leu1-32 ade6-210*
Genetic reagent (*S. pombe*)	*car2* mutant	This manuscript	FC 3348	*car2∆::kanMX4 arg1-230 lys3-37*
Genetic reagent (*S. pombe*)	*car2* mutant, *cdc25* mutant	This manuscript	FC 3349	*cdc25-22 car2∆::kanMX4 arg1-230 lys3-37*
Genetic reagent (*S. pombe*)	*car2* mutant, *wee1* mutant	This manuscript	FC 3350	*wee1-50 car2∆::kanMX4 arg1-230 lys3-37*
Chemical compound/drug	YES 225 Media	Sunrise Science Production	#2011	
Chemical compound/drug	Edinburgh Minimum Media (EMM)	MP Biomedicals	#4110-32	
Chemical compound/drug	Agar			
Chemical compound/drug	Histidine	Sigma-Aldrich	#H8000	
Chemical compound/drug	Uracil	Sigma-Aldrich	#U0750	

Reagent type (species) or resource	Designation	Source or reference	Identifiers	Additional Information
Chemical compound/drug	Adenine	Sigma-Aldrich	#A9126	
Chemical compound/drug	Thiamine	Sigma-Aldrich	#T4625	
Chemical compound/drug	Dimethyl sulfoxide (DMSO)	Fisher Scientific	#67-68-5	
Chemical compound/drug	1-NM-PP1	Fisher Scientific	#50-203-0494	
Chemical compound/drug	Agarose	Invitrogen	#16500500	
Chemical compound/drug	Dulbecco's Phosphate Buffer Saline	Thermo Scientific	14190144	
Chemical compound/drug	4% formaldehyde (methanol-free)	Thermo Scientific	#28,906	
Chemical compound/drug	RNAse A	Thermo Scientific	#EN0531	
Chemical compound/drug	Fluorescin isothiocyanate isomer I	Sigma	#F7250	
Chemical compound/drug	Light arginine (L-ARGININE:HCL–Unlabeled)	Cambridge Isotope Laboratories	#ULM-8347-PK	
Chemical compound/drug	Heavy arginine (L-ARGININE:HCL(13C6,99%))	Cambridge Isotope Laboratories	#CNLM-2265-H-0.25	
Chemical compound/drug	Light lysine (L-LYSINE:2HCL–Unlabeled)	Cambridge Isotope Laboratories	#ULM-8766-PK	
Chemical compound/drug	Heavy lysine (L-LYSINE:2HCL(4,4,5,5-D4,96-98%))	Cambridge Isotope Laboratories	#DLM-2640-0.5	
Chemical compound/drug	Iodoacetamide	Sigma	#I1149-5G	
Chemical compound/drug	TPCK-treated trypsin	Worthington	#LS003740	
Chemical compound/drug	Sep-Pak 50mg C18 column	Waters	##054955	

Reagent type (species) or resource	Designation	Source or reference	Identifiers	Additional Information
Software, algorithm	µManager v. 1.41	Edelstein et al., 2010; Edelstein et al., 2014		
Software, algorithm	Mathworks	Mathworks	2018a	
Software, algorithm	Python	Drake Jr. and Van Rossum, 1995	3.8.8	
Software, algorithm	Prism	GraphPad	Version 9.4.1	
Software, algorithm	FIJI ImageJ	Schindelin et al., 2012		
Software, algorithm	MaxQuant (v2.4.2)			
Other	µ-Slide VI 0.4 channel slide	Ibidi	#80606	

Yeast strains and media

Schizosaccharomyces pombe strains were constructed and maintained using standard methods (Forsburg, 2003). The strains used in this study are listed in Table 4.1. For expression of 40nm cytGEMs, yeast cells were transformed with the plasmid pREP41X-PfV-mSapphire for expression of the protein fusion PfV encapsulin-mSapphire (Delarue *et al.*, 2018; Lemière *et al.*, 2022; Garner *et al.*, 2023). These cells were grown in EMM3S (minus leucine) media with 0.1µg/mL thiamine for an intermediate level of expression from the nmt1* promoter to optimize the appropriate numbers of cytGEMs in each cell (Maundrell, 1993; Molines *et al.*, 2022). In other experiments, cells were grown in rich YES (Fig. 2.5) or SILAC adjusted EMM media (Fig. 2.6).

Temperature shift and inhibitor treatments

Fission yeast cells of different cell sizes and ploidy were generated using established conditional cell cycle mutants (see main text). For temperature-shift experiments (Figs. 2.1 A-D, 2.3) wildtype and temperature-sensitive mutant cells were inoculated from colonies freshly grown from the frozen stocks on EMM3S (minus leucine) agar plates grown at 25°C for 3 days and stored at room temp for less than 7 days. Cells were inoculated in liquid EMM3S medium and grown at 25°C with shaking for over 12 hours to exponential phase in the range of OD_{600} 0.2 to 0.6. The flasks were then transferred to a 36°C shaking incubator for the indicated period (3-6 hours). The cells were then harvested and mounted in chambers for imaging on the lab bench and promptly returned to 36°C in the pre-warmed microscope system incubator. No significant differences in cytGEMs diffusion were found when mounting cells on the bench at room temperature (~5 minutes of preparation time) versus preparing cells inside the temperature-controlled cage installed on the microscope. For experiments at semi-permissive temperatures (Fig. S1), cells were maintained at a steady temperature (25-30°C) for ~18 hours and imaged at the indicated temperature in the incubator. For inhibition of cdc2-as and sid2-as alleles (Figs. 2.1, 2.2, 2.3, 2.4), cells were grown in liquid EMM3S at 30°C with shaking and treated with 10μM 1-NM-PP1 (100-fold dilution of a 4mM stock in DMSO) (#50-203-0494, #67-68-5, Fisher Scientific) for 3-6 hours. Cells were harvested and imaged as above.

Preparation of cells for live cell microscopy

Cells were placed just before imaging into μSlide VI 0.4 channel slides (#80606, Ibidi – 6 channels slide, channel height 0.4mm, length 17mm, and width 3.8mm, tissue culture

treated and sterilized). The μSlide was first pre-coated by incubation with 100μg/mL of lectin (#L1395, Sigma) for at least 15 min at room temperature and then removed from the chamber. For mounting cells, 1 mL of liquid yeast culture was centrifuged for 2 minutes in an microcentrifuge tube at 400 x G at room temperature. Most supernatant was removed, and the cell pellet was gently resuspended in the remaining ~100 μL media. 50 μL of this concentrated cell mixture was added the pre-coated chamber and allowed to adhere for 2 minutes and washed three times with pre-warmed media to remove non-adhered cells.

Microscopy

For imaging of cytGEMs (Fig. 2.1 and 2.3), live cells were imaged with a TIRF Diskovery system (Andor) with a Ti-Eclipse 2 inverted microscope stand (Nikon Instruments), 488nm laser illumination, a 60X TIRF oil objection (NA: 1:49, oil DIC N2) (#MRD01691, Nikon), and a sCMOS camera (Zyla, Andor). These components were controlled with μManager v. 1.41 (Edelstein et al., 2010; Edelstein et al., 2014). Temperature was maintained by a black panel cage incubation system (#748-3040, OkoLab). Cells were mounted in μSlide VI 0.4 channel slides (#80606, Ibidi – 6 channels slide, channel height 0.4mm, length 17mm, and width 3.8mm, tissue culture treated and sterilized).

For imaging of nuclei and fluorescence intensity quantification (Fig. 2.3 and 2.5), cells were imaged on a Ti-Eclipse inverted microscope (Nikon Instruments) with a spinning-disk confocal system (Yokogawa CSU-10) that includes 488nm and 541nm laser illumination (with Borealis) and emission filters 525±25nm and 600±25nm respectively, 40X (NA: 0.6) and 60X (NA: 1.4) objectives, and an EM-CCD camera (Hamamatsu,

C9100-13). These components were controlled with μManager v. 1.41 (Edelstein *et al.*, 2010, 2014). Temperature was maintained by a black panel cage incubation system (#748–3040, OkoLab).

Imaging and analysis of cytGEMs

Cells expressing cytGEMs nanoparticles were imaged in fields of 1K x 1.2K pixels or smaller using highly inclined laser beam illumination at 100Hz for 5 seconds. Cells generally exhibited 10-20 of cytGEMs particles/cell. CytGEMs were tracked with the ImageJ (Schindelin *et al.*) particle Tracker 2D-3D tracking algorithm from MosaicSuite (Sbalzarini and Koumoutsakos, 2005) with the following parameters: run("Particle Tracker 2D/3D", "radius = 3 cutoff= 0 per/abs = 0.03 link = 1 displacement = 6 dynamics = Brownian"). In Figures 1-2, GEMs were analyzed collectively in multiple cells in the whole field of view. For analyses of individual cells (Fig. 2.1 D), cells were individually cropped from field images, and cytGEMs were tracked with the same MosaiSuite parameters with the exception of per/abs = 0.03. The analyses of the cytGEMs tracks were as described in Delarue et al., 2018, with methods to compute mean square displacement (MSD) using MATLAB (MATLAB_R2018, MathWorks). The effective diffusion coefficient Deff was obtained by fitting the first 10 time points of the MSD curve (MSDtruncated) to the canonical 2D diffusion law for Brownian motion: $MSD_{truncated}(\tau)=4 \cdot D_{eff} \cdot \tau$.

Measurement of cell length and nuclei count

As a proxy for cell size, cell length along the long axis of the rod-shaped cells was measured manually using ImageJ Line Selection tool on brightfield images of cells.

“Straight Line” or “Segmented Line” was used depending on cell morphology. For determination of the number of nuclei, strains with the nuclear envelope marker Ish1 tagged with a fluorescent protein were grown in EMM3S (minus leucine) media, and number of nuclei were counted manually. Septated-cells were excluded from analysis.

Ribosomal concentration quantification

Ribosomal concentration was measured in individual fission yeast cells using a ribosomal protein Rps2-GFP signal intensity, similarly as described (Knapp et al., 2019; Lemière et al., 2022). Cells expressing Rps2-GFP were grown in rich YES liquid media at 25°C overnight and shifted to 36°C for 6 hours before imaging. Cells were mounted on a 2% agarose (#16500500, Invitrogen) in YES 225 (#2011, Sunrise Science Production) pad and imaged with 488 nm laser illumination via spinning disk confocal microscopy. The Rps2-GFP signal was acquired in 500 nm z-step stacks, and a sum of stack of the middle 3 slices was used for intensity quantification. For each selected cell, the Rps2-GFP signal intensities were measured along the long cell axis (averaged over 4 μm in width) and normalized by cell length. The signal was corrected for background intensity and uneven illumination of the field. Rps2-GFP signals were defined as the average of the mean signal between 0.2-0.3 and the mean signal between 0.7–0.8 (peak signals in the cytoplasm, avoiding the nucleus) along the normalized cell length. Finally, all Rps2-GFP signals were normalized to the mean of the cell length (L) category $9 \leq L < 18$ μm.

Cellular protein concentration quantification

Total protein was measured in individual fission yeast cells using FITC staining, similarly as described (Knapp *et al.*, 2019b; Odermatt *et al.*, 2021; Lemière *et al.*, 2022). Cells were grown in YES liquid media at 25°C overnight and shifted to 36°C for 6 hours until fixation. 1 mL of exponential-phase (OD_{600} = 0.2-0.6) cell culture was fixed with 4% final concentration formaldehyde (methanol-free 37% solution, #28906, Thermo Scientific, Waltham) and incubated at 4°C overnight. Fixed cells were washed 3 times with phosphate buffered saline (PBS) (#14190, Thermo Scientific) and resuspended in 100 µL of PBS. 100 µL of fixed cells were treated with 0.1 mg/mL RNAse A (#EN0531, Thermo Scientific) and incubated in a rotator for 2 hours at 37°C. Next, cells were washed and re-suspended in PBS and stained with 50 ng/mL FITC (#F7250, Sigma) for 30 min, washed three times with PBS, and resuspended in PBS. Cells were mounted on a 2% agarose (#16500500, Invitrogen) in Dulbecco's Phosphate Buffer Saline (Thermo Scientific, 14190144) pad and imaged with 488 nm laser illumination via spinning disk confocal microscopy. FITC signal was acquired and analyzed using similar methods as the Rps2-GFP experiments described above.

LC-MS/MS sample preparation

Proteomic experiments were performed using stable isotope labeling by amino acids in cell culture (SILAC) (Ong *et al.*, 2002). SILAC-compatible fission yeast strains containing car2Δ were grown in SILAC adjusted media (Edinburgh Minimal Media (#4110712, MP Biomedicals) + 6 mM ammonium chloride + 0.04 mg/ml arginine and 0.03 mg/ml lysine) using either light or ‘‘heavy’’ versions of Lysine and Arginine (Swaffer *et al.*, 2016). The

“light” (Agr0 Lys0) version of the media contained L-Arginine and L-Lysine built with normal 12C and 14N isotopes; the “heavy" (Arg6 Lys4) version had L-Arginine containing six 13C atoms and L-Lysine containing four deuterium atoms. For SILAC experiments, cells were grown for at least 8 generations at the indicated temperatures 25-36°C with shaking before collection, diluted in the morning and evening so they are always below OD_{600} = 0.3. The mean cell volume for proteomics samples was determined by Z2 Coulter Counter (Beckman Coulter), and the mean cell volumes of these samples matched those of the corresponding samples used in the cytGEMs experiments.

10 mL of fission yeast cultures were pelleted by centrifugation at 3,000 x G for 2 minutes at 4°C. The supernatant was removed, and cell pellets were snap frozen in liquid nitrogen and stored at -80°C. Frozen pellets were resuspended in 300 µL of yeast lysis buffer (50mM Tris, 150mM NaCl, 5mM EDTA, 0.2% Tergitol, pH 7.5 ; + a cOmplete ULTRA Tablet) with 700µL of glass beads. Lysis was performed at 4°C in a MPBio Fastprep24 (4 cycles with the following settings: 6.0 m/s, 40 seconds). Cell lysates were cleared by centrifugation at 12,000 x G for 5 minutes at 4°C. Protein concentration was quantified using a Pierce BCA Protein Assay Kit (Prod# 23255). Equal amounts of protein from each SILAC-labeled lysate were mixed. The mixed lysates were then denatured/reduced in 1% SDS and 10mM DTT (15 minutes at 65°C), alkylated with 5mM iodoacetamide (15 minutes at room temperature), and then precipitated with three volumes of a solution containing 50% acetone and 50% ethanol (on ice for 10 minutes). Proteins were re-solubilized in 2M urea, 50mM Tris-HCl, pH 8.0, and 150mM NaCl, and then digested with TPCK-treated trypsin (50:1) overnight at 37°C. Trifluoroacetic acid and formic acid were added to the digested peptides for a final concentration of 0.2% (pH ~3). Peptides were

desalted with a Sep-Pak 50 mg C18 column (Waters). The C18 column was conditioned with 500 µL of 80% acetonitrile and 0.1% acetic acid and then washed with 1000 µL of 0.1% trifluoroacetic acid. After samples were loaded, the column was washed with 2000 µL of 0.1% acetic acid followed by elution with 400 µL of 80% acetonitrile and 0.1% acetic acid. The elution was dried in a Concentrator at 45°C.

LC-MS/MS data acquisition

Desalted SILAC-labeled peptides were analyzed on a Fusion Lumos mass spectrometer (Thermo Fisher Scientific, San Jose, CA) equipped with a Thermo EASY-nLC 1200 LC system (Thermo Fisher Scientific, San Jose, CA). Peptides were separated by capillary reverse phase chromatography on a 25 cm column (75 µm inner diameter, packed with 1.6 µm C18 resin, AUR2-25075C18A, Ionopticks, Victoria Australia). Peptides were introduced into the Fusion Lumos mass spectrometer using a 125 minute stepped linear gradient at a flow rate of 300 nL/minute. The steps of the gradient are as follows: 3–27% buffer B (0.1% (v/v) formic acid in 80% acetonitrile) for 105 minutes, 27-40% buffer B for 15 minutes, 40-95% buffer B for 5 minutes, and finally maintained at 90% buffer B for 5 minutes. Column temperature was maintained at 50°C throughout the procedure. Xcalibur software (Thermo Fisher Scientific) was used for the data acquisition and the instrument was operated in data-dependent mode. Advanced peak detection was enabled. Survey scans were acquired in the Orbitrap mass analyzer (Profile mode) over the range of 375 to 1500 m/z with a mass resolution of 240,000 (at 200 m/z). For MS1, the Normalized AGC Target (%) was set at 250 and max injection time was set to “Auto”. Selected ions were fragmented by Higher-energy Collisional Dissociation (HCD) with

normalized collision energies set to 31, and the fragmentation mass spectra were acquired in the Ion trap mass analyzer with the scan rate set to “Turbo”. The isolation window was set to 0.7 m/z window. For MS2, the Normalized AGC Target (%) was set to “Standard” and max injection time was set to “Auto”. Repeated sequencing of peptides was kept to a minimum by dynamic exclusion of the sequenced peptides for 30 seconds. Maximum duty cycle length was set to 1 second.

Spectral searches

All raw files were searched using the Andromeda engine (Cox et al., 2011) embedded in MaxQuant (v1.6.7.0) (Cox and Mann, 2008). In brief, 2-label SILAC search was conducted using MaxQuant’s default Arg6/10 and Lys4/8. Variable modifications included oxidation (M) and protein N-terminal acetylation, and carbamidomthyl (C) was a fixed modification. The number of modifications per peptide was capped at 5. Digestion was set to tryptic (proline-blocked). Peptides were ‘‘Re-quantified’’, and maxquant’s match-between-runs feature was not enabled. Database search was conducted using the UniProt proteome - UP000002485. Minimum peptide length was 7 amino acids. FDR was determined using a reverse decoy proteome (Elias and Gygi, 2007).

Peptide quantitation

Our SILAC analysis utilized MaxQuant’s ‘‘proteinGroups.txt’’ output file. Contaminant and decoy peptide identifications were discarded. When applicable, the “Leading Razor Protein” designation was used to assign non-unique peptides to individual proteins.

Normalized SILAC ratios were used to determine changes in the relative concentrations of individual proteins.

Protein annotations

Protein annotations in Figure 4 were sourced from UniProt columns named “Gene Ontology IDs” “Subcellular localization [CC]” or PomBase “Complex Annotations” unless otherwise noted (Rutherford *et al.*; UniProt: the Universal Protein Knowledgebase in 2023 The UniProt Consortium, 2022). Protein localization was strictly parsed so that each annotated protein belongs to only one of the designated groups. Proteins with 2 or more annotations were ignored (except for the “Cytoplasm/Nucleus” category which required a nuclear and cytoplasmic annotation and for categories, e.g. Histone, Chromosome, Nucleolus, which also contained a “Nucleus” annotation).

Gene ontology enrichment analysis

Relative protein concentration ratios were averaged between the two repetitions of proteomics experiments. Under- and overrepresented proteins were defined as having a minimum of a 10% change in their mean relative protein concentration ratio. GO process characterization of protein lists was performed using Protein Analysis Through Evolutionary Relationships (PANTHER) overrepresentation analysis version PANTHER 18.0 (Thomas *et al.*, 2022).

Ortholog analysis

Human ortholog pairs were retrieved using the DRSC Integrative Ortholog Prediction Tool (DIOPT) found at https://www.flyrnai.org/cgi-bin/DRSC_orthologs.pl. *S. pombe* proteins

were used as the “input” species and humans were set as the “output”. Only ortholog pairs with a DIOPT “weighted Score” of greater than 10 were considered for our analyses. Once *S. pombe* proteins were matched with a human ortholog protein, we imported protein slope values derived for human RPE-1 cell line from Lanz et al. 2021.

References

1. Amodeo, AA, Jukam, D, Straight, AF, and Skotheim, JM (2015). Histone titration against the genome sets the DNA-to-cytoplasm threshold for the Xenopus midblastula transition. Proc Natl Acad Sci U S A 112, E1086–E1095.
2. Aoi, Y, Kawashima, SA, Simanis, V, Yamamoto, M, and Sato, M (2014). Optimization of the analogue-sensitive Cdc2/Cdk1 mutant by in vivo selection eliminates physiological limitations to its use in cell cycle analysis. Open Biol 4.
3. Balachandra, S, Sarkar, S, and Amodeo, AA (2022). The Nuclear-to-Cytoplasmic Ratio: Coupling DNA Content to Cell Size, Cell Cycle, and Biosynthetic Capacity. Annu Rev Genet 56, 165–185.
4. Basier, C, and Nurse, P (2023). The cell cycle and cell size influence the rates of global cellular translation and transcription in fission yeast. EMBO J 42.
5. Bellotto, N, Agudo-Canalejo, J, Colin, R, Golestanian, R, Malengo, G, and Sourjik, V (2022). Dependence of diffusion in Escherichia coli cytoplasm on protein size, environmental conditions, and cell growth. Elife 11.
6. Cadart, C, and Heald, R (2022). Scaling of biosynthesis and metabolism with cell size. Mol Biol Cell 33, pe5.
7. Chadwick, WL, Biswas, SK, Bianco, S, and Chan, YHM (2020). Non-random distribution of vacuoles in Schizosaccharomyces pombe. Phys Biol 17.
8. Chen, D, Toone, WM, Mata, J, Lyne, R, Burns, G, Kivinen, K, Brazma, A, Jones, N, and Bähler, J (2003). Global transcriptional responses of fission yeast to environmental stress. Mol Biol Cell 14, 214–229.

9. Claude, K-L, Bureik, D, Chatzitheodoridou, D, Adarska, P, Singh, A, and Schmoller, KM Transcription coordinates histone amounts and genome content.
10. Cox, J, and Mann, M (2008). MaxQuant enables high peptide identification rates, individualized p.p.b.-range mass accuracies and proteome-wide protein quantification. Nat Biotechnol 26.
11. Creanor, J, and Mitchison, JM (1982). Patterns of protein synthesis during the cell cycle of the fission yeast Schizosaccharomyces pombe. J Cell Sci 58, 263–285.
12. Delarue, M, Brittingham, GP, Pfeffer, S, Surovtsev, I V., Pinglay, S, Kennedy, KJ, Schaffer, M, Gutierrez, JI, Sang, D, Poterewicz, G, *et al.* (2018). mTORC1 Controls Phase Separation and the Biophysical Properties of the Cytoplasm by Tuning Crowding. Cell 174, 338-349.e20.
13. Demidenko, ZN, and Blagosklonny, M V. (2008). Growth stimulation leads to cellular senescence when the cell cycle is blocked. Cell Cycle 7, 3355–3361.
14. Edelstein, A, Amodaj, N, Hoover, K, Vale, R, and Stuurman, N (2010). Computer control of microscopes using manager. Curr Protoc Mol Biol.
15. Edelstein, AD, Tsuchida, MA, Amodaj, N, Pinkard, H, Vale, RD, and Stuurman, N (2014). Advanced methods of microscope control using μManager software. Journal of Biological Methods | 1, 10.
16. Elias, JE, and Gygi, SP (2007). Target-decoy search strategy for increased confidence in large-scale protein identifications by mass spectrometry.
17. Elliott, SG (1983). Coordination of growth with cell division: Regulation of synthesis of RNA during the cell cycle of the fission yeast Schizosaccharomyces pombe. MGG Molecular & General Genetics 192, 204–211.

18. Elliott, SG, Warner, JR, and McLaughlin, CS (1979). Synthesis of ribosomal proteins during the cell cycle of the yeast Saccharomyces cerevisiae. J Bacteriol 137, 1048–1050.
19. Facchetti, G, Knapp, B, Flor-Parra, I, Chang, F, and Howard, M (2019). Reprogramming Cdr2-Dependent Geometry-Based Cell Size Control in Fission Yeast. Current Biology 29, 350-358.e4.
20. Fantes, PA, and Nurse, P (1978). Control of the timing of cell division in fission yeast. Cell size mutants reveal a second control pathway. Exp Cell Res 115, 317–329.
21. Forsburg, SL (2003). Growth and Manipulation of S. pombe . Curr Protoc Mol Biol 64.
22. Garner, RM, Molines, AT, Theriot, JA, and Chang, F (2023). Vast heterogeneity in cytoplasmic diffusion rates revealed by nanorheology and Doppelgänger simulations. Biophys J 122, 767–783.
23. Ginzberg, MB, Kafri, R, and Kirschner, M (2015). On being the right (cell) size. Science (1979) 348.
24. Grallert, A, Connolly, Y, Smith, DL, Simanis, V, and Hagan, IM (2012). The S. pombe cytokinesis NDR kinase Sid2 activates Fin1 NIMA kinase to control mitotic commitment through Pom1/Wee1. Nat Cell Biol.
25. Hachet, O, Berthelot-Grosjean, M, Kokkoris, K, Vincenzetti, V, Moosbrugger, J, and Martin, SG (2011). A Phosphorylation Cycle Shapes Gradients of the DYRK Family Kinase Pom1 at the Plasma Membrane. Cell 145, 1116–1128.

26. Hagan, IM, Grallert, A, and Simanis, V (2016). Synchronizing Progression of Schizosaccharomyces pombe Cells from G2 through Repeated Rounds of Mitosis and S Phase with cdc25-22 Arrest Release. Cold Spring Harb Protoc 2016, pdb.prot091264.
27. Hecht, VC, Sullivan, LB, Kimmerling, RJ, Kim, DH, Hosios, AM, Stockslager, MA, Stevens, MM, Kang, JH, Wirtz, D, Vander Heiden, MG, *et al.* (2016). Biophysical changes reduce energetic demand in growth factor–deprived lymphocytes. Journal of Cell Biology 212, 439–447.
28. Heimlicher, MB, Bächler, M, Liu, M, Ibeneche-Nnewihe, C, Florin, EL, Hoenger, A, and Brunner, D (2019). Reversible solidification of fission yeast cytoplasm after prolonged nutrient starvation. J Cell Sci 132.
29. Joyner, RP, Tang, JH, Helenius, J, Dultz, E, Brune, C, Holt, LJ, Huet, S, Müller, DJ, and Weis, K (2016). A glucose-starvation response regulates the diffusion of macromolecules. Elife 5.
30. Kawashima, SA, Chen, Z, Aoi, Y, Patgiri, A, Kobayashi, Y, Nurse, P, and Kapoor, TM (2016). Potent, Reversible, and Specific Chemical Inhibitors of Eukaryotic Ribosome Biogenesis. Cell 167, 512-524.e14.
31. Keifenheim, D, Sun, X-M, Mayhew, MB, Marguerat, S, and Correspondence, NR (2017). Size-Dependent Expression of the Mitotic Activator Cdc25 Suggests a Mechanism of Size Control in Fission Yeast. Current Biology 27.
32. Knapp, BD, Odermatt, P, Rojas, ER, Cheng, W, He, X, Huang, KC, Correspondence, FC, Edu, K, and Chang, F (2019a). Decoupling of Rates of Protein Synthesis from Cell Expansion Leads to Supergrowth Article Decoupling

of Rates of Protein Synthesis from Cell Expansion Leads to Supergrowth. Cell Syst 9, 434–445.

33. Knapp, BD, Odermatt, P, Rojas, ER, Cheng, W, He, X, Huang, KC, Correspondence, FC, Edu, K, and Chang, F (2019b). Decoupling of Rates of Protein Synthesis from Cell Expansion Leads to Supergrowth Article Decoupling of Rates of Protein Synthesis from Cell Expansion Leads to Supergrowth. Cell Syst 9, 434–445.
34. Lanz, MC, Zatulovskiy, E, Swaffer, MP, Zhang, L, Ilerten, I, Zhang, S, You, DS, Marinov, G, McAlpine, P, Elias, JE, *et al.* (2022). Increasing cell size remodels the proteome and promotes senescence. Mol Cell 82, 3255-3269.e8.
35. Lanz, MC, Zhang, S, Swaffer, MP, Ziv-Uziel, I, Hernendez-Gotz, L, Jaroz, DF, Elias, JE, Skotheim, JM, and Zuckerberg Biohub San Francisco, C (2023). Genome dilution by cell growth drives starvation-like proteome remodeling in mammalian and yeast cells. BioRxiv, 2023.10.16.562558.
36. Lemière, J, Real-Calderon, P, Holt, LJ, Fai, TG, and Chang, F (2022). Control of nuclear size by osmotic forces in Schizosaccharomyces pombe. Elife 11, 1–41.
37. Lengefeld, J, Cheng, C-W, Maretich, P, Blair, M, Hagen, H, McReynolds, MR, Sullivan, E, Majors, K, Roberts, C, Ho Kang, J, *et al.* (2021). Cell size is a determinant of stem cell potential during aging. Sci Adv 7, 271.
38. Lloyd, AC (2013). The Regulation of Cell Size. Cell 154, 1194–1205.
39. Marguerat, S, and Bähler, J (2012). Coordinating genome expression with cell size. Trends in Genetics 28, 560–565.

40. Marshall, WF (2020). Scaling of Subcellular Structures. Annu Rev Cell Dev Biol 36, 219–236.
41. Martin, SG, and Berthelot-Grosjean, M (2009). Polar gradients of the DYRK-family kinase Pom1 couple cell length with the cell cycle. Nature.
42. Maundrell, K (1993). Thiamine-repressible expression vectors pREP and pRIP for fission yeast. Gene 123, 127–130.
43. Mitchison, TJ (2019). Colloid osmotic parameterization and measurement of subcellular crowding. Mol Biol Cell 30, 173–180.
44. Molines, AT, Lemière, J, Gazzola, M, Steinmark, IE, Edrington, CH, Hsu, CT, Real-Calderon, P, Suhling, K, Goshima, G, Holt, LJ, *et al.* (2022). Physical properties of the cytoplasm modulate the rates of microtubule polymerization and depolymerization. Dev Cell 57, 466-479.e6.
45. Moseley, JB, Mayeux, A, Paoletti, A, and Nurse, P (2009). A spatial gradient coordinates cell size and mitotic entry in fission yeast. Nature 2009 459:7248 459, 857–860.
46. Mu, L, Kang, JH, Olcum, S, Payer, KR, Calistri, NL, Kimmerling, RJ, Manalis, SR, and Miettinen, TP (2020). Mass measurements during lymphocytic leukemia cell polyploidization decouple cell cycle- And cell size-dependent growth. Proc Natl Acad Sci U S A 117, 15659–15665.
47. Munder, MC, Midtvedt, D, Franzmann, T, Nüske, E, Otto, O, Herbig, M, Ulbricht, E, Müller, P, Taubenberger, A, Maharana, S, *et al.* (2016). A pH-driven transition of the cytoplasm from a fluid- to a solid-like state promotes entry into dormancy. Elife 5.

48. Neumann, FR, and Nurse, P (2007). Nuclear size control in fission yeast. Journal of Cell Biology 179, 593–600.

49. Neurohr, GE, and Amon, A (2020). Relevance and Regulation of Cell Density. Trends Cell Biol 30, 213–225.

50. Neurohr, GE, Terry, RL, Lengefeld, J, Bonney, M, Brittingham, GP, Moretto, F, Miettinen, TP, Vaites, LP, Soares, LM, Paulo, JA, *et al.* (2019). Excessive Cell Growth Causes Cytoplasm Dilution And Contributes to Senescence. Cell 176, 1083-1097.e18.

51. Nurse, P (1975). Genetic control of cell size at cell division in yeast. Nature 256, 547–551.

52. Nurse, P (1985). Cell cycle control genes in yeast. Trends in Genetics 1, 51–55.

53. Nurse, P, Thuriaux, P, and Nasmyth, K (1976). Genetic control of the cell division cycle in the fission yeast Schizosaccharomyces pombe. MGG Molecular & General Genetics 146, 167–178.

54. Odermatt, PD, Miettinen, TP, Lemière, J, Kang, JH, Bostan, E, Manalis, SR, Huang, KC, and Chang, F (2021). Variations of intracellular density during the cell cycle arise from tip-growth regulation in fission yeast. Elife 10, 1–23.

55. Ong, S-E, Blagoev, B, Kratchmarova, I, Kristensen, DB, Steen, H, Pandey, A, and Mann, M (2002). Stable Isotope Labeling by Amino Acids in Cell Culture, SILAC, as a Simple and Accurate Approach to Expression Proteomics*. Molecular & Cellular Proteomics 1, 376–386.

56. Padovan-Merhar, O, Nair, GP, Biaesch, AG, Mayer, A, Scarfone, S, Foley, SW, Wu, AR, Churchman, LS, Singh, A, and Raj, A (2015). Single Mammalian Cells

Compensate for Differences in Cellular Volume and DNA Copy Number through Independent Global Transcriptional Mechanisms. Mol Cell 58, 339–352.

57. Persson, LB, Ambati, VS, and Brandman, O (2020). Cellular Control of Viscosity Counters Changes in Temperature and Energy Availability. Cell 183, 1572-1585.e16.
58. Pickering, M, Hollis, LN, D'Souza, E, and Rhind, N (2019). Fission yeast cells grow approximately exponentially. Cell Cycle 18, 869–879.
59. Rivas, G, and Minton, AP (2016). Macromolecular Crowding In Vitro, In Vivo, and In Between. Trends Biochem Sci 41, 970–981.
60. Rutherford, KM, Lera-Ramírez, M, and Wood, V PomBase: a Global Core Biodata Resource-growth, collaboration, and sustainability.
61. Sakai, K, Kondo, Y, Goto, Y, and Aoki, K (2023). Cytoplasmic fluidization triggers breaking spore dormancy in fission yeast. BioRxiv, 2023.09.27.559686.
62. Sbalzarini, IF, and Koumoutsakos, P (2005). Feature point tracking and trajectory analysis for video imaging in cell biology.
63. Schindelin, J, Arganda-Carreras, I, Frise, E, Kaynig, V, Longair, M, Pietzsch, T, Preibisch, S, Rueden, C, Saalfeld, S, Schmid, B, *et al.* Fiji-an Open Source platform for biological image analysis.
64. Schizosaccharomyces, I, and Mitchison, PJM (1957). THE GROWTH OF SINGLE CELLS. Exp Cell Res 13, 244–262.
65. Schmoller, KM, Turner, JJ, Kõivomägi, M, and Skotheim, JM (2015). Dilution of the cell cycle inhibitor Whi5 controls budding-yeast cell size. Nature 2015 526:7572 526, 268–272.

66. Shi, H, Hu, Y, Odermatt, PD, Gonzalez, CG, Zhang, L, Elias, JE, Chang, F, and Huang, KC Precise regulation of the relative rates of surface area and volume synthesis in bacterial cells growing in dynamic environments.
67. Sidell, BD, and Hazel, JR (1987). Temperature affects the diffusion of small molecules through cytosol of fish muscle. J Exp Biol 129, 191–203.
68. Sun, XM, Bowman, A, Priestman, M, Bertaux, F, Martinez-Segura, A, Tang, W, Whilding, C, Dormann, D, Shahrezaei, V, and Marguerat, S (2020). Size-Dependent Increase in RNA Polymerase II Initiation Rates Mediates Gene Expression Scaling with Cell Size. Current Biology 30, 1217-1230.e7.
69. Swaffer, MP, Jones, AW, Flynn, HR, Snijders, AP, and Nurse, P (2016). CDK Substrate Phosphorylation and Ordering the Cell Cycle. Cell 167, 1750-1761.e16.
70. Swaffer, MP, Marinov, GK, Zheng, H, Fuentes Valenzuela, L, Tsui, CY, Jones, AW, Greenwood, J, Kundaje, A, Greenleaf, WJ, Reyes-Lamothe, R, *et al.* (2023). RNA polymerase II dynamics and mRNA stability feedback scale mRNA amounts with cell size. Cell 186, 5254-5268.e26.
71. Szórádi, T, Shu, T, Kidiyoor, GR, Xie, Y, Herzog, NL, Bazley, A, Bonucci, M, Keegan, S, Saxena, S, Ettefa, F, *et al.* nucGEMs probe the biophysical properties of the nucleoplasm.
72. Tai, YT, Fukuda, T, Morozumi, Y, Hirai, H, Oda, AH, Kamada, Y, Akikusa, Y, Kanki, T, Ohta, K, and Shiozaki, K (2023). Fission Yeast TORC1 Promotes Cell Proliferation through Sfp1, a Transcription Factor Involved in Ribosome Biogenesis. Mol Cell Biol 43, 675–692.

73. Thomas, PD, Ebert, D, Muruganujan, A, Mushayahama, T, Albou, LP, and Mi, H (2022). PANTHER: Making genome-scale phylogenetics accessible to all. Protein Science 31, 8–22.
74. Urgen Cox, J, Neuhauser, N, Michalski, A, Scheltema, RA, Olsen, J V, and Mann, M (2011). Andromeda: A Peptide Search Engine Integrated into the MaxQuant Environment. J Proteome Res 10.
75. Wood, E, and Nurse, P (2015). Sizing up to Divide: Mitotic Cell-Size Control in Fission Yeast. Annu Rev Cell Dev Biol 31, 11–29.
76. Xie, S, Swaffer, M, and Skotheim, JM (2022). Eukaryotic Cell Size Control and Its Relation to Biosynthesis and Senescence. Annu Rev Cell Dev Biol 38, 291–319.
77. Zatulovskiy, E, and Skotheim, JM (2020). On the Molecular Mechanisms Regulating Animal Cell Size Homeostasis. Trends in Genetics 36, 360–372.
78. Zhou, H-X, Rivas, G, and Minton, AP (2008). Macromolecular Crowding and Confinement: Biochemical, Biophysical, and Potential Physiological Consequences. Annu Rev Biophys 37, 375–397.
79. Zhurinsky, J, Leonhard, K, Watt, S, Marguerat, S, Bähler, J, and Nurse, P (2010). A coordinated global control over cellular transcription. Current Biology 20, 2010–2015.
80. (2022). UniProt: the Universal Protein Knowledgebase in 2023 The UniProt Consortium. Nucleic Acids Res 51, 523–531.

Publishing Agreement

It is the policy of the University to encourage open access and broad distribution of all theses, dissertations, and manuscripts. The Graduate Division will facilitate the distribution of UCSF theses, dissertations, and manuscripts to the UCSF Library for open access and distribution. UCSF will make such theses, dissertations, and manuscripts accessible to the public and will take reasonable steps to preserve these works in perpetuity.

I hereby grant the non-exclusive, perpetual right to The Regents of the University of California to reproduce, publicly display, distribute, preserve, and publish copies of my thesis, dissertation, or manuscript in any form or media, now existing or later derived, including access online for teaching, research, and public service purposes.

DocuSigned by:
Catherine Tan
D7CFD59A8F6246B...
Author Signature

5/20/2024
Date